

Rakel Sæter Heggset

Test of a centrifugal pump

Master's thesis in Mechanical Engineering

Supervisor: Bjørn Winther Solemslie

June 2020

NTNU
Norwegian University of Science and Technology
Faculty of Engineering
Department of Mechanical and Industrial Engineering



Norwegian University of
Science and Technology

Rakel Sæter Heggset

Test of a centrifugal pump

Thesis for the degree of Mechanical Engineering

Trondheim, June 2020

Norwegian University of Science and Technology
Faculty of Engineering Science and Technology
Department of Energy and Process Engineering



EPT-M-2020

MASTEROPPGAVE

for

Student Rakel Heggset

Våren 2020

Test av en sentrifugalpumpe*Test of a centrifugal pump***Bakgrunn**

Den raske utviklingen i batterier og elektriske motorer de siste årene gjør at stadig flere pumper elektrifiseres der forbrenningsbaserte løsninger tidligere var brukt. Elektrisk utstyr er typisk mer fleksibelt, rimeligere og tryggere. I mange tilfeller betyr dette også kortere utviklingstider og lavere kostnader, noe som gjør at elektriske pumper nå finner stadig flere bruksområder. I enkelte bruksområder er vekt et viktig kriterium, og man vil da ønske å ha relativt høy rotasjonshastighet, noe som gir utfordringer i både utvikling og testing.

Det er gjennomført et design av en høyhastighets sentrifugalpumpe i tidligere arbeid, og i denne oppgaven vil det fokuseres på test av denne pumpe.

Mål

Gjennomføre hydraulisk virkningsgradsmåling av en sentrifugalpumpe

Oppgaven bearbejdes ut fra følgende punkter:

1. Litteraturstudie
 - a. Hydraulisk og mekanisk design av sentrifugalpumper
 - b. Test av sentrifugalpumper
2. Software kunnskap
 - a. DAK-programmet CREO eller SolidWorks
 - b. Labview og Matlab
3. Målinger av sentrifugalpumpe i Vannkraftlaboratoriet
 - a. Virkningsgradsmålinger
 - b. Trykkpulsasjonsmålinger (og vibrasjonsmålinger hvis mulig)
 - c. Temperaturmålinger
4. Dersom studenten skal dra til Nepal på ekskursjon så skal tidligere arbeid fra prosjektet og det videre arbeidet i denne hovedoppgaven bli skrevet som en egen publikasjon og presentert på konferansen: 10th International symposium on Current Research in Hydraulic Turbines (CRHT-X) ved Kathmandu University 31. mars 2020.

” - ”

Senest 14 dager etter utlevering av oppgaven skal kandidaten levere/sende instituttet en detaljert fremdrift- og eventuelt forsøksplan for oppgaven til evaluering og eventuelt diskusjon med faglig ansvarlig/veiledere. Detaljer ved eventuell utførelse av dataprogrammer skal avtales nærmere i samråd med faglig ansvarlig.

Besvarelsen redigeres mest mulig som en forskningsrapport med et sammendrag både på norsk og engelsk, konklusjon, litteraturliste, innholdsfortegnelse etc. Ved utarbeidelsen av teksten skal kandidaten legge vekt på å gjøre teksten oversiktlig og velskrevet. Med henblikk på lesning av

besvarelsen er det viktig at de nødvendige henvisninger for korresponderende steder i tekst, tabeller og figurer anføres på begge steder. Ved bedømmelsen legges det stor vekt på at resultatene er grundig bearbeidet, at de oppstilles tabellarisk og/eller grafisk på en oversiktlig måte, og at de er diskutert utførlig.

Alle benyttede kilder, også muntlige opplysninger, skal oppgis på fullstendig måte. For tidsskrifter og bøker oppgis forfatter, tittel, årgang, sidetall og eventuelt figurnummer.

Det forutsettes at kandidaten tar initiativ til og holder nødvendig kontakt med faglærer og veileder(e). Kandidaten skal rette seg etter de reglementer og retningslinjer som gjelder ved alle (andre) fagmiljøer som kandidaten har kontakt med gjennom sin utførelse av oppgaven, samt etter eventuelle pålegg fra Institutt for energi- og prosesseteknikk.

Risikovurdering av kandidatens arbeid skal gjennomføres i henhold til instituttets prosedyrer. Risikovurderingen skal dokumenteres og inngå som del av besvarelsen. Hendelser relatert til kandidatens arbeid med uheldig innvirkning på helse, miljø eller sikkerhet, skal dokumenteres og inngå som en del av besvarelsen. Hvis dokumentasjonen på risikovurderingen utgjør veldig mange sider, leveres den fulle versjonen elektronisk til veileder og et utdrag inkluderes i besvarelsen.

I henhold til ”Utfyllende regler til studieforskriften for teknologistudiet/sivilingeniørstudiet” ved NTNU § 20, forbeholder instituttet seg retten til å benytte alle resultater og data til undervisnings- og forskningsformål, samt til fremtidige publikasjoner.

Besvarelsen leveres digitalt i DAIM. Et faglig sammendrag med oppgavens tittel, kandidatens navn, veileders navn, årstall, instituttnavn, og NTNUs logo og navn, leveres til instituttet som en separat pdf-fil. Etter avtale leveres besvarelse og evt. annet materiale til veileder i digitalt format.

- Arbeid i Vannkraftlaboratoriet
 Feltarbeid

NTNU, Institutt for energi- og prosesseteknikk, 10. juni 2020

Bjørn W. Solemslie
Bjørn Winther Solemslie
Faglig ansvarlig/veileder

Medveileder: Ole Gunnar Dahlhaug
Eivind Liland

Preface

This master's thesis was conducted at the Waterpower Laboratory at NTNU Gløshaugen during the spring semester of 2020 as a continuation of the project thesis completed during the fall semester of 2019. The main work this year has been to prepare and carry out hydraulic efficiency measurements of an electric centrifugal pump.

After many hours in the laboratory, I have learned a great deal about calibration and measurement procedures and how to operate with hydraulic turbomachines. This experience has given me greater insight into hydropower and its importance, an insight that is very much appreciated. I also got to learn how to use SolidWorks during the fall semester, which was very exciting.

I am grateful for the opportunity to write a master's thesis at the Waterpower Laboratory. The experience has given me a broad range of knowledge, and the atmosphere in the laboratory is something special. I especially consider the informality of exchanging knowledge between professors, technicians, and students throughout this project, as highly valuable. It has been a pleasure to collaborate with both fellow students and employees at the Waterpower Laboratory during this demanding yet fun year.



Rakel Heggset
Trondheim, June 2020

Acknowledgements

I would like to express my gratitude to my supervisor during this master's thesis, Bjørn Winther Solemslie, for his patience during numerous discussions, and his advice and guidance on how to solve this task.

Johannes Kverno, I would like to thank for his many hours of helping out in the laboratory with calibration and measurement procedures. I would also like to thank Bård Brandåstrø for his advice regarding implementations of the test rig, and especially Joard Grilstad, for his many hours spent carrying out these implementations.

Also, a thank you to Gro Mari Langleite for her close collaboration during this semester, for sharing her knowledge and discussing solutions to different arising problems. At last, I would like to express my appreciation to all my fellow students at the Waterpower Laboratory for making this year a really good one.

Abstract

In this thesis, a centrifugal pump meant for electric engines has been examined. Battery technology and electronic equipment have experienced significant progress in the last years and made it possible to replace the more traditional gas turbine pumps. An electrified pump comes with the advantage of being more flexible, cheaper, and safer, and has a more versatile design. The cooperating company in this study aims to verify the design for their first prototype of an electrical centrifugal pump. The area of application requires considerably high rotational speeds, and the pump is designed for 10 000 *rpm*. The optimal inlet and outlet pressure is 5 *bar* and 20 *bar*, respectively. Hence, the objective of this thesis has been to perform hydraulic efficiency measurements of the centrifugal pump, conducted at the Waterpower Laboratory at NTNU.

The measurements were carried out by running the pump at a constant rotational speed for the entire flow range to obtain the pump characteristics. As the test rig was a new installation in the laboratory, the pump was initially tested at low rotational speeds before testing closer to design point. The tests only reached approximately 3000 *rpm* before cracks appeared in the pump casing near the outlet, leakage originated from the cracks, and the testing had to be stopped. The highest measured efficiency was 42.29% and was assumed to be low, considering the pump was operating far from the design point. Another issue during the tests was the negative pressure difference across the pump inlet and outlet, resulting in negative head and efficiency for higher flow rates.

It has been concluded that the pump design is not verified due to failure at a pressure lower than designed parameters. Therefore, a decent amount of time has been spent working out possible improvements and a strategy for further work. The tests should be repeated after the recommended changes are carried out, to draw further conclusions about the pump characteristics and efficiencies at designed conditions.

Sammendrag

I dette prosjektet har en sentrifugalpumpe for elektriske motorer blitt undersøkt. En rask progresjon innen batteriteknologi og elektrisk utstyr de siste årene, har gjort det mulig å erstatte de mer tradisjonelle gassturbin-pumpene med elektriske pumper. Slike pumper er typisk mer fleksible, billigere og tryggere, samt enklere for parametrisk skalering. Samarbeidsselskapet for dette prosjektet ønsker å verifisere designet for sin første prototype av en elektrisk sentrifugalpumpe. Dens bruksområde krever en betraktelig høy rotasjonshastighet og er designet for 10 000 *rpm*. Det optimale inn- og utløpstrykk er henholdsvis 5 *bar* og 20 *bar*. Målet med denne oppgaven har dermed vært å gjennomføre hydrauliske virkningsgradsmålinger av sentrifugalpumpen, utført i Vannkraftlaboratoriet på NTNU.

Målingene ble utført ved å kjøre pumpen på et konstant turtall og variere volumstrømmen, fra null til maksimal volumstrøm, for å oppnå pumpekararakteristikken. Fordi testriggen var en ny installasjon i laboratoriet, ble pumpen først testet ved lave turtall før kjøring nærmere optimalt turtall. Testen nådde bare omtrent 3000 *rpm* før det oppstod sprekker i pumpehuset nært utløpet. Det oppstod lekkasje fra sprekken og testingen måtte stoppes. Den høyeste målte virkningsgraden var 42.29 % og er antatt å være rimelig lav da pumpen opererte langt unna optimalt driftspunkt. Et annet problem som ble oppdaget underveis i testingen var en negativ trykkforskjell fra pumpens innløp til utløp. Dette resulterte i en negativ løftehøyde og virkningsgrad for høyere volumstrøm.

Det har blitt konkludert at pumpedesignet ikke er verifisert på grunn av svikt under kjøreforhold med lavere trykk enn det pumpen er designet for. Derfor har det blitt lagt ned mye arbeid ved å utarbeide mulig forbedringer og en strategi videre arbeid. Testene bør gjentas etter de anbefalte endringene er gjennomført, og slik kan videre konklusjoner for pumpekararakteristikken og virkningsgraden for optimale betingelser bestemmes.

Contents

Preface	i
Acknowledgements	iii
Abstract	v
Sammendrag	vii
Contents	ix
List of Tables	xvii
List of Figures	xxi
List of Symbols	xxiii
1 Introduction	1
1.1 Background	1
1.2 Objective	2
1.3 Previous work	2
1.3.1 Nils Marius Sakserud: CFD analysis	2

1.3.2	Company of collaboration: Pump design	2
1.3.3	Project thesis: Test rig design	3
2	Theoretical background	5
2.1	Centrifugal pumps	5
2.1.1	Pump components	5
2.1.2	Velocity triangles	6
2.2	Energy transfer	7
2.2.1	Power	7
2.2.2	Head	7
2.3	Pump performance	9
2.3.1	Losses	9
2.3.2	Hydraulic efficiency	9
2.3.3	Pump characteristics	10
2.3.4	Affinity laws	12
2.4	Flow phenomena	13
2.4.1	Cavitation	13
	Consequences of cavitation	13
	Cavitation assessment	13
2.4.2	Pressure pulsations	14
	Frequencies	15
	Analysing pressure pulsations	16
2.5	Uncertainty in experiments	16
2.5.1	Spurious errors	16
2.5.2	Random errors	16
2.5.3	Systematic errors	17

2.5.4	Regression error	17
3	Test rig setup	19
3.1	Waterpower Laboratory	19
3.1.1	Lower water reservoir	19
3.1.2	Feed pumps	19
3.1.3	Loop configurations	20
3.1.4	Pressure tank	20
3.2	Rig design	21
3.2.1	Base design	21
3.2.2	Belt drive	21
3.2.3	Brackets	22
3.2.4	V- clamps	22
3.2.5	Setup for cooling	22
3.2.6	Valve	23
3.3	Instrumentation	24
3.3.1	Pressure	24
3.3.2	Volume flow rate	24
3.3.3	Torque	25
3.3.4	Rotational speed	25
3.4	Rig setup in the laboratory	26
4	Experimental methods and calibration	29
4.1	Calibration	29
4.1.1	Linear regression	29
4.1.2	Calibration of the pressure transducers	30

4.1.3	Calibration of the flow meter	32
4.1.4	Calibration of the torque transducer	34
4.2	Experimental method	35
4.2.1	Test procedure	35
4.2.2	Post-processing	35
4.2.3	Correction of outlet pressure	35
4.2.4	Rapid prototyping	36
	Procedure for 3D-printing	36
	Filament	36
5	Uncertainty analysis	37
5.1	Uncertainty in calibration	37
5.1.1	Uncertainty in the calibration of pressure transducers	38
5.1.2	Uncertainty in the calibration of flow meter	39
5.1.3	Uncertainty in the calibration of torque transducer	40
5.2	Uncertainty in the measurements	40
5.2.1	Uncertainty in the pressure measurements	41
5.2.2	Uncertainty in the flow rate measurements	42
5.2.3	Uncertainty in the torque measurements	42
5.2.4	Uncertainty in the rotational speed measurements	43
5.3	Uncertainty of the hydraulic efficiency	43
6	Results	45
6.1	Results from the measurements	45
6.1.1	HQ-curves	45
6.1.2	Hydraulic efficiency	48

6.1.3	Pressure drop in 90° bend	49
6.1.4	Observations during testing	51
6.2	3D printed impeller	51
7	Discussion	53
7.1	Discussion of the measurements	53
7.1.1	HQ-curves	53
7.1.2	Affinity laws	54
7.1.3	Hydraulic efficiency	54
7.1.4	Pressure drop in 90° bend	55
7.2	Discussion of uncertainty analysis	55
7.3	Discussion of possible improvements	57
7.3.1	Centrifugal pump	57
	Impeller	57
	Casing	57
	Leakage	57
7.3.2	Test rig	58
	Torque measurement	58
	Installation of outlet pressure transducer	58
	Manual valve	58
	Detection of cavitation	58
8	Conclusion	59
9	Further work	61
9.1	Future testing	61
9.2	Evaluation of flow phenomena	62

References	63
A Calibration procedures	65
A.1 Calibration procedure for weighing tank	66
A.2 Calibration procedure for flow meter	69
A.3 Calibration procedure for torque transducer	73
A.4 Calibration of pressure transducers	77
B Results	83
B.1 Pressure drop in 90° bend	83
C Uncertainty analysis	87
C.1 Uncertainty in the calibration	87
C.1.1 Uncertainty in the calibration of flow meter	87
C.1.2 Uncertainty in the calibration of torque transducer	88
C.2 Uncertainty in the measurements	88
C.2.1 Uncertainty of the hydraulic efficiency	88
D Procedure for running the Centrifugal Pump Test Rig	91
D.1 General	91
D.2 The system	91
D.2.1 Description	91
D.2.2 Equipment used for testing	91
D.3 Operation	92
D.3.1 Initial setting of the pipe system	92
D.3.2 Preparations	92
Setting up the system	92

	Starting the pump and filling the pressure tank	92
	Starting the engine	93
D.3.3	Run the test	93
	Measuring the HQ-curve	93
D.3.4	Shut down	94
	Turning off engine	94
	Draining the pressure tank	94
	Shutting down	94
	Emergency shut down	94
D.4	Figures	95
E	Procedure for 3D printing	99
F	MatLab codes	101

List of Tables

2.1	Cavitation criteria [1].	14
5.1	Error components in the calibration procedure.	37
5.2	Uncertainty in the calibration of the pressure transducer.	39
5.3	Uncertainty in the calibration of the flow meter.	39
5.4	Uncertainty in the calibration of the torque transducer.	40
5.5	Error components from tests.	41
5.6	Uncertainty in the pressure measurements.	42
5.7	Uncertainty in the volume flow rate measurements.	42
5.8	Uncertainty in the torque measurements.	43
6.1	Test matrix for the measurements.	46
6.2	Deviation between measured head and head found with affinity laws.	48
6.3	BEP for each rotational speed obtained from the measurements.	49
D.1	Status for valves in the pipe system before starting procedure.	97

List of Figures

1.1	Pump design, obtained from SolidWorks.	3
1.2	Cross sections of the pump, obtained from SolidWorks.	3
1.3	Final rig design, obtained from SW.	4
2.1	The components of a centrifugal pump [1].	6
2.2	General velocity triangles on the leading edge and trailing edge of the impeller.	6
2.3	H-Q curve for a pump [2].	10
2.4	Regulation of rotational speed with efficiency curves [3].	12
2.5	Cutwater in the volute casing.	15
3.1	Loop configurations in the Waterpower Laboratory [4].	20
3.2	Initial rig setup.	21
3.3	Installation of belt drive system and brackets.	22
3.4	V- clamps at the inlet and outlet.	23
3.5	Setup for cooling of bearings.	23
3.6	Installation of pressure transducer on the outlet pipe.	24
3.7	Optiflux 2300C with an IFC 300 signal converter.	25

3.8	Torque transducer and rotational speed instrumentation.	26
3.9	Schematic of the rig setup in the Waterpower Laboratory.	27
4.1	Calibration curve for the inlet pressure transducer with a total error band scaled by 100.	31
4.2	Calibration curve for the outlet pressure transducer with a total error band scaled by 100.	31
4.3	Calibration curve for the electromagnetic flow meter with a total error band scaled by 10.	33
4.4	Calibration curve for the weighing tank.	33
4.5	Calibration curve for the torque transducer with a total error band scaled by 100.	34
6.1	HQ-curves obtained from testing.	47
6.2	Data points scaled using the affinity laws.	47
6.3	The measured HQ-curve compared to the fitted line using the affinity laws.	48
6.4	Efficiency curves approximated from measured data.	49
6.5	Relative deviation for the head.	50
6.6	Measured and corrected HQ-curves compared for 2176 <i>rpm</i>	50
6.7	3D printing of the impeller.	51
7.1	Errors present when calibrating the flow meter.	56
B.1	Comparison of HQ-curves with measured outlet pressure vs. corrected pressure for 1206 <i>rpm</i>	83
B.2	Comparison of efficiency with measured outlet pressure vs. corrected pressure for 1896 <i>rpm</i>	84
B.3	Comparison of efficiency with measured outlet pressure vs. corrected pressure for 2176 <i>rpm</i>	84

B.4	Comparison of efficiency with measured outlet pressure vs. corrected pressure for <i>2928rpm</i>	85
D.1	Ventilation and frequency drive.	95
D.2	Starting the engine.	95
D.3	Valves	96
D.4	Manual valve on lower part of the pressure tank	96

List of Symbols

Latin Symbols

A	Area	m^2
a	Calibration constant	
B	Blade width	m
b	Calibration constant	
B	Geometry shape factor	—
c	Absolute velocity	m/s
c_m	Meridian component of absolute velocity	m/s
c_s	Velocity at suction side	m/s
D	Diameter	m
E	Energy	J/kg
e_X	Absolute error of some quantity X	
F	Force	N
f	Friction factor	—
f_{max}	Maximum expected frequency	Hz
f_{Ny}	Nyquist frequency	Hz
f_X	Relative error of some quantity X	

f_s	Sampling frequency	Hz
f_v	von Karman frequency	Hz
g	Gravitational constant	m/s^2
H	Head	m
k_b	Bend loss coefficient	
k_1	Friction loss coefficient	s^2/m^5
k_2	Impact loss coefficient	s^2/m^5
L	Length	m
m	Mass	kg
MV	Measured value	
N	Number of blades	
n	Number of measurements	
n	Rotational speed	rpm
p	Pressure	Pa
P_h	Hydraulic power	W
P_m	Mechanical power	W
p_s	Suction pressure	Pa
p_v	Vapor pressure	Pa
Q	Volume flow rate	m^3/s
r	Radius	m
R_b	Bend radius	m
Re	Reynolds number	—
S_Y	Standard deviation	
S_{XX}	Error variation of input around linear approximation	
S_{XY}	Error co-variation of output and input around linear approximation	

S_{YY}	Error variation of output around linear approximation	
St	Strouhal number	–
T	Torque	Nm
t	Blade thickness	m
t	t-value	–
u	Peripheral velocity	m/s
U	Mean flow velocity	m/s
W	Weight	kg
w	Relative velocity	m/s
x	Blade length	m
Y	Measured quantity	
Z	Height	m
z	Height coordinate	m

Greek Symbols

α	Absolute blade angle	$^{\circ}$
β	Relative blade angle	$^{\circ}$
δ	Boundary layer thickness	m
Δ	Difference	–
η	Efficiency	–
γ	Slip coefficient	–
ρ	Fluid density	kg/m^3
ω	Angular velocity	rad/s

Abbreviation

BEP	Best Efficiency Point
CFD	Computational Fluid Dynamics

NPSH	Net Positive Suction Head
NTNU	Norwegian University of Science and Technology
RSS	Root-sum-square
RSI	Rotor-Stator Interaction
SSE	Sum square error
STL	Stereolithography
SW	SolidWorks

Indices

1	Inlet
2	Outlet
∞	Infinite number of blades
<i>amb</i>	Ambient
<i>atm</i>	Atmospheric
<i>A</i>	Available
<i>cal</i>	Calibration
<i>h</i>	Hydraulic
<i>i</i>	Data point
<i>l</i>	Leakage
<i>m</i>	Mechanical
<i>opt</i>	Optimal
<i>r</i>	Required
<i>t</i>	Theoretical
<i>u</i>	Circumferential velocity component
<i>w</i>	Water

Chapter I

Introduction

1.1 Background

In the early 19th century, the first centrifugal pumps driven by slow-speed engines only applied to areas of application for low heads. Due to the low pump efficiency at this time, the method was considered uneconomic. When Osborn Reynolds produced the first turbine pump in 1875, in which the impeller delivered the water to guide vanes, the efficiency increased considerably. Nowadays, pumps have been manufactured for almost every possible duty for transportation or raising the pressure of liquids, and the centrifugal pumps are one of the most applied pumps in the industry. Their area of application is typically, but not exclusively, transportation or removal of water, circulation of water for heat withdrawal, increase of liquid pressure, and storage of water in elevated reservoirs [5].

The recent years rapid development in battery technology and electrical engines, has enabled the use of electrified pumps as a replacement for the more traditional steam turbine pumps. Electrical equipment is usually more flexible, cheaper, and safer with a shorter production time, but will have an additional weight due to the battery. An electrical centrifugal pump will have a more versatile design, which makes it possible to use one design for different kinds of engines. The only parameters changing are the pressure, the volume flow rate, and the fuel density.

Investigated in this thesis is an electric centrifugal pump meant for transporting fuel into a combustion chamber and is powered by a battery-driven engine. The pump is designed and produced by a Norwegian company, which desires to verify the design and its performance. The name of the company is not included in this thesis due to confidentiality.

1.2 Objective

The objective of this thesis is to perform hydraulic efficiency measurements of the centrifugal pump using the facilities in the Waterpower Laboratory at NTNU Gløshaugen. The work includes establishing the pump characteristics at different operational points presented in an H-Q diagram and determine the hydraulic efficiency. An examination of pressure pulsations, vibrations, and temperatures are also included for this study.

1.3 Previous work

In this section, previous work related to the centrifugal pump will be presented. It includes previous CFD analysis from a master student at the Waterpower Laboratory, the finalized pump design done by the company of collaboration, and the design of the test rig.

1.3.1 Nils Marius Sakserud: CFD analysis

In his master's thesis, Nils Marius Sakserud carried out a CFD analysis of the centrifugal pump on a first draft design. The requirement for an approved pump design was no presence of cavitation and achieving the desired pressure. The impeller simulation showed promising results, although this is expected in CFD due to a smooth impeller surface. On the other hand, the requirements for the entire pump design were not reached, and the volute losses remained unknown [6].

As for further work, Sakserud suggested in his conclusion to complete a full CFD analysis of the pump, including the inlet, impeller, volute, and outlet in order to determine the overall hydraulic performance. The CFD analysis did not proceed as the pump design was already finished when starting this thesis.

1.3.2 Company of collaboration: Pump design

The centrifugal pump to be tested in this study is the first prototype of its kind and can be seen in Figure 1.1. The centrifugal pump is a single-stage, single-entry pump with a volute casing. It is manufactured in aluminum and designed for a rotational speed of 10 000 *rpm* and a volume flow rate of 25 *l/s*. The intended inlet pressure is 5 *bar*, but it is desired to investigate the possibility for a lower inlet pressure before cavitation arises. The set outlet pressure is 20 *bar*.

Figure 1.2(a) shows the front view cross-section of the pump and the enclosed impeller with six blades, or runner vanes. Figure 1.2(b) shows the shaft going through two ball bearings, located close to the impeller, installed to reduce rotational friction and support radial and axial loads. In the back, the pump casing is

equipped with three ports for cooling the seals and ball bearings. The coolant will be the operational fluid.

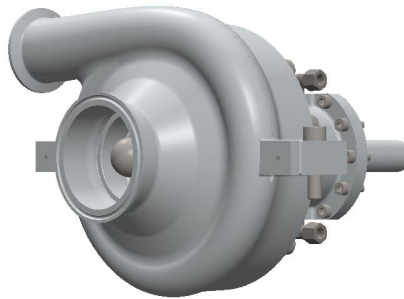
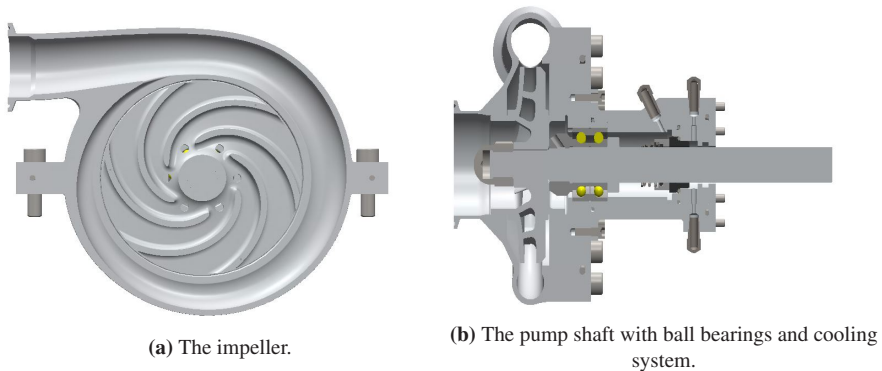


Figure 1.1: Pump design, obtained from SolidWorks.



(a) The impeller.

(b) The pump shaft with ball bearings and cooling system.

Figure 1.2: Cross sections of the pump, obtained from SolidWorks.

1.3.3 Project thesis: Test rig design

The centrifugal pump test rig was designed as part of the author's project thesis during the fall semester of 2019, using SolidWorks (SW). An existing test rig at the Waterpower Laboratory was used as a base, consisting of a red plate welded onto a steady frame. The rig also contained an electric engine, a torque transducer, and a bearing block.

In order to achieve desired rotational speed at the impeller, it was necessary to assembly a geared belt drive system to the rig. The system consist of one small and one large gear drive, and a rubber belt. The rubber belt transfers the mechanical

power from the large to the small gear drive and increases the rotational speed of the impeller shaft with a ratio of 8.

Figure 1.3 shows the final rig design. Brackets and bearing blocks were designed in order to mount the pump to the plate in a horizontally aligned position. Also, the figure illustrates the pipes for inlet and outlet. The water enters from above the rig, flows through the pump, and continues down into the lower water reservoir.

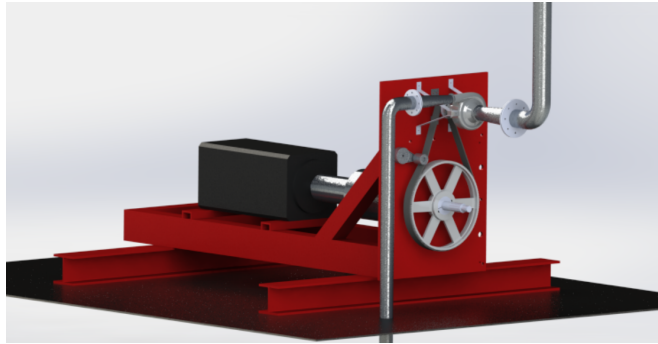


Figure 1.3: Final rig design, obtained from SW.

Chapter II

Theoretical background

When performing the experiment and evaluating the resulting measured data, the theory behind centrifugal pumps should be appreciated. This chapter provides an insight into the theory for centrifugal pump and the relevant performance data. Important hydraulic phenomena arising during pump operation, such as cavitation and pressure pulsations, are also included. The end of this chapter introduces the theory behind the uncertainty related to this experiment.

2.1 Centrifugal pumps

Centrifugal pumps are considered necessary in many areas of the industry, both from a technical and an economic perspective. Their area of application ranges from central heating pumps of a few watts to large storage pumps and pump turbines operating at several megawatts. The flow rate for a centrifugal pump can vary from 0.0001 to 60 m^3/s , heads ranging from 1 to 5000 m , and the rotational speed can differ between a few hundred to 30 000 revolutions per minute [1]. Common for all centrifugal pumps is the conversion of mechanical power, provided by an engine or an electric motor, into hydraulic power by utilizing centrifugal forces.

2.1.1 Pump components

The structure of a centrifugal pump consists mainly of the suction eye and outlet, the impeller and the volute casing as shown in Figure 2.1. First, the fluid enters the pump through the suction eye with an axial direction, flows through the impeller, and accelerates in the circumferential direction. The impeller is connected to the engine shaft and converts the mechanical energy to hydraulic energy. When leaving the impeller, the flow enters the volute casing. The volute is a curved channel with an increasing cross-sectional area approaching the outlet, which builds a pressure increase of the flow and decelerates the flow velocity. At last, the flow exits the

pump through the outlet [1].

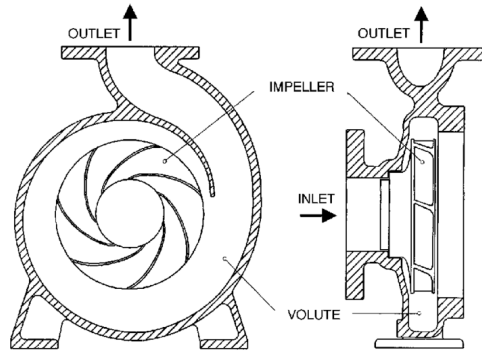


Figure 2.1: The components of a centrifugal pump [1].

2.1.2 Velocity triangles

In order to understand the behavior of the flow through the pump, it is convenient to study the velocity triangles related to the inlet and outlet flow. The velocity triangles are considered at the leading edge, and the trailing edge of the impeller and the velocities involved are the relative velocity, w , the peripheral velocity, $u = \omega \times r$, and the absolute velocity, $c = u + w$.

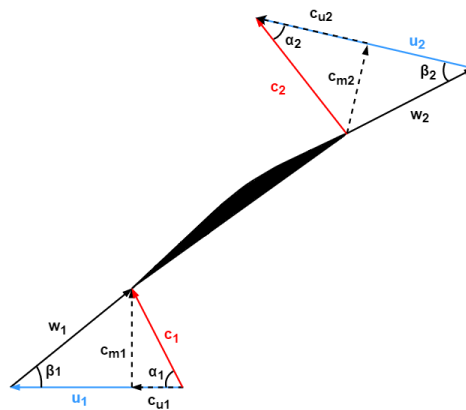


Figure 2.2: General velocity triangles on the leading edge and trailing edge of the impeller.

Inlet velocity triangle: The fluid entering the impeller is mostly axial, which for this case, makes the blade angle in the absolute reference frame at the inlet, α_1 , equal to 90° . Hence, the circumferential component of the absolute inflow velocity becomes $c_{u1} = 0$. The meridian velocity at the leading edge is related to the volume flow rate and the inlet area by $c_{m1} = Q/A_1$ [1]. Shown in Figure 2.2, the inlet velocities are denoted with subscript 1.

Outlet velocity triangle: As the fluid flows through the impeller runner vanes, energy is transmitted from the blades to the fluid through pressure forces. The pressure forces cause a slip condition at the outlet, meaning the relative velocity is no longer aligned with the blade angle β . The angle deviation between the blade angle and the relative velocity caused by the slip conditions is defined as the slip angle $\Delta\beta$ [3]. In Figure 2.2, the outlet velocities are denoted with subscript 2.

2.2 Energy transfer

2.2.1 Power

The centrifugal pump is a *shaft power receiving turbomachine*, i.e., an external motor is driving the machine. In such machines, the energy is supplied to the fluid by the rotor, or more specific, the impeller [7]. The mechanical power supplied, P_m , is defined by the torque, T , and the angular velocity, ω , of the engine shaft, as expressed in Equation 2.1.

$$P_m = T \cdot \omega \quad [W] \quad (2.1)$$

The power transferred from the impeller to the flow is the hydraulic power, denoted as P_h . The hydraulic power is the output power of the centrifugal pump and is defined in Equation 2.2. Due to hydraulic losses in the pump, the mechanical power must exceed the hydraulic power. The losses concerning the hydraulic power are further elaborated in section 2.3.

$$P_h = \rho \cdot g \cdot H \cdot Q \quad [W] \quad (2.2)$$

2.2.2 Head

A common way to measure energy transfer in centrifugal pumps is by the term head, which is a measure of the useful energy transmitted from the pump to the fluid between the inlet and outlet. The head is expressed in fluid column height, as shown in Equation 2.3 .

$$H = \frac{p_2 - p_1}{\rho \cdot g} + \frac{c_2^2 - c_1^2}{2 \cdot g} + (z_2 - z_1) \quad [m] \quad (2.3)$$

Here, p denotes the static pressure, c denotes the velocity, and z denotes the height coordinate. Subscripts 1 and 2 refers to the pump inlet and outlet, respectively [1].

If no losses were present in the impeller, considering an infinite number of blades with zero thickness, the outlet velocity would be blade-congruent with zero slip. The head is then referred to as the *theoretical head* and is denoted $H_{t\infty}$. The torque transferred from the impeller blades to the water equals $F \cdot r$, where r is the impeller radius. The force, F , is expressed in terms of the mass flow rate, \dot{m} , and the circumferential component of the absolute velocity, as shown in Equation 2.4. When defining $\dot{m} = \rho \cdot Q$, the torque transferred between the inlet and outlet can be expressed as in Equation 2.5

$$F = \dot{m} \cdot c_{u\infty} \quad [N] \quad (2.4)$$

$$T = \rho \cdot Q \cdot (r_2 \cdot c_{u2\infty} - r_1 \cdot c_{u1\infty}) \quad [Nm] \quad (2.5)$$

Further, the energy transferred, $E_{t\infty}$, to the flow is expressed in terms of the mechanical power introduced in Equation 2.1. By using the definition of the torque and expressing the angular velocity as $\omega = u/r$, the mechanical power and the energy becomes:

$$P_m = \rho \cdot Q \cdot (u_2 \cdot c_{u2\infty} - u_1 \cdot c_{u1\infty}) \quad [W] \quad (2.6)$$

$$E_{t\infty} = \frac{P_m}{\rho \cdot Q} = (u_2 \cdot c_{u2\infty} - u_1 \cdot c_{u1\infty}) \quad [J/kg] \quad (2.7)$$

With the head equal to E/g , Equation 2.8 defines the theoretical head with an infinite number of blades and no losses.

$$H_{t\infty} = \frac{u_2 \cdot c_{u2\infty} - u_1 \cdot c_{u1\infty}}{g} \quad [m] \quad (2.8)$$

Equation 2.8 is referred to as the *Euler's pump equation* and shows that the head is independent of the fluid density. The pump will produce the same head when transporting water, mercury, or air. When considering the slip angle described in section subsection 2.1.2, going from an infinite to a finite number of blades, the expression for the theoretical head is [3]:

$$H_t = \frac{u_2 \cdot c_{u2} - u_1 \cdot c_{u1}}{g} \quad [m] \quad (2.9)$$

2.3 Pump performance

2.3.1 Losses

Losses occur when a fluid flows through a machine, and therefore, the hydraulic power is consequently smaller compared to the mechanical power provided by the engine. Brekke [3] defines the losses present in a centrifugal pump, as described below.

Hydraulic losses: Includes all the losses in the flow between the suction eye and the outlet. Hydraulic losses are generated through friction and vortex dissipation. When the fluid flows through the impeller, the flow experience a rapid change in direction between the blades and leads to impact losses. Another contribution is the friction losses that occur due to friction between the water and solid surfaces in the pump. Hydraulic losses also include rotational losses, arising when the pump is operating outside its best operational point.

Volumetric and disk friction losses: Because of the running clearance between the impeller and the pump casing, there will be an amount of flow leakage. Hence, the flow rate will be lower than the designed flow rate. The required flow rate can then be expressed as $Q_r = Q + Q_l$, where Q_l denotes the rate of leakage flow. In addition to the leakage losses, losses due to disk friction between the impeller and the casing are present.

Mechanical losses: The mechanical losses are generated by the radial and axial bearings and the shaft seals, and by other mechanical forces acting on the system while running.

2.3.2 Hydraulic efficiency

The hydraulic efficiency is the ratio between the output and input power, respectively, and for power receiving turbomachines, this equals the ratio between the hydraulic power and the mechanical power. Thus, the pump efficiency can be expressed as shown in Equation 2.10 [2].

$$\eta_h = \frac{\text{Hydraulic power}}{\text{Mechanical power}} = \frac{P_h}{P_m} \quad [-] \quad (2.10)$$

By using the definition of the hydraulic and mechanical power described in subsection 2.2.1 the efficiency can be rewritten as:

$$\eta_h = \frac{\rho \cdot g \cdot H \cdot Q}{T \cdot \omega} \quad [-] \quad (2.11)$$

For specific operating conditions, the pump efficiency achieves a maximum value, referred to as the Best Efficiency Point (BEP) [1].

2.3.3 Pump characteristics

A useful tool to understand the performance characteristics during distinct operational points is the pump performance curve. A performance characteristic means the relationship between two operational quantities. Typically recognized for the characteristics of centrifugal pumps, is the relation between the head and the volume flow rate, while operating the pump at one constant rotational speed [7].

The performance curve for centrifugal pumps is referred to as the H - Q curve and describes the head as a function of the flow rate. The H - Q curve, illustrated in Figure 2.3, defines the behaviour of the head over the total flow range. All pumps temporarily operate away from their designed flow, defined as *Q , and represent the BEP. At lower values than *Q , the flow is denoted part load, while higher flow rates are denoted overload.

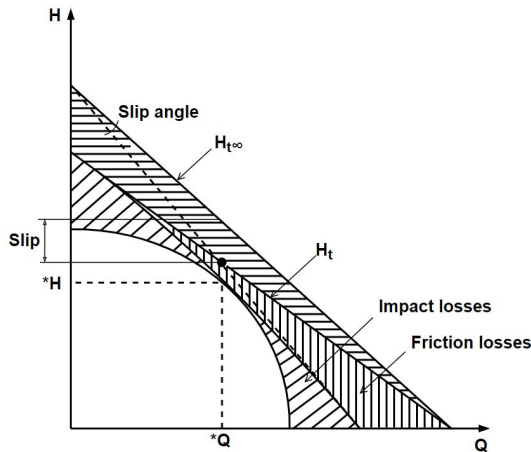


Figure 2.3: H - Q curve for a pump [2].

The HQ -curve can be distinguished from the Euler pump equation introduced in subsection 2.2.2. When considering zero losses in the pump and an infinite number of blades, an ideal curve is defined by $H_{t\infty}$ and draws the top linear line in Figure 2.3. By using the outlet velocity diagram, the expression of the circumferential component of the absolute velocity is the following:

$$\begin{aligned} c_{u2\infty} &= u_2 - w_{u2} \quad [m/s] \\ c_{u2\infty} &= u_2 - \frac{c_{m2}}{\tan\beta_{2\infty}} \quad [m/s] \end{aligned} \quad (2.12)$$

c_{m2} is the axial component of the outlet velocity and is proportional with the flow rate. Defining the outlet area as $A_2 = \pi \cdot D_2 \cdot B_2$, where D_2 is the impeller outlet diameter and B_2 is the blade outlet width, one can write c_{m2} as in Equation 2.13.

$$c_{m2} = \frac{Q}{A_2} = \frac{Q}{\pi \cdot D_2 \cdot B_2} \quad [m/s] \quad (2.13)$$

When assuming designed conditions at $c_{u1} = 0$, a new expression for the ideal pump curve can be rewritten by including the velocities defined in Equation 2.12 and Equation 2.13:

$$H_{t\infty} = \frac{u_2}{g} \cdot \left(u_2 - \frac{Q}{\pi \cdot D_2 \cdot B_2 \cdot \tan\beta_{2\infty}} \right) \quad [m] \quad (2.14)$$

Considering the slip condition and a finite number of blades, the head drops from $H_{t\infty}$ to H_t . The line for the theoretical head after considering the slip condition is shown in Figure 2.3. Gülich [1] introduces a slip factor, denoted γ , which defines $(1 - \gamma)$ as the slip magnitude. The slip is related to the velocities as shown in Equation 2.15.

$$c_{u2\infty} - c_{u2} = (1 - \gamma) \cdot u_2 \quad (2.15)$$

Rearranging Equation 2.15 into an expression for c_{u2} , the theoretical head based on the Euler pump equation with slip condition becomes:

$$H_t = \frac{u_2 \cdot c_{u2}}{g} = \frac{u_2}{g} \cdot \left(u_2 \cdot \gamma - \frac{Q}{\pi \cdot D_2 \cdot B_2 \cdot \tan\beta_{2\infty}} \right) \quad [m] \quad (2.16)$$

The slip factor ranges from $0 \leq \gamma \leq 1$, where $\gamma = 1$ equals blade-congruent flow. A smaller γ indicates a greater slip angle.

The curve for the actual head, H , is found by subtracting the hydraulic losses from the H_t -line. For the HQ-curve, the hydraulic losses include the friction and impact losses. Additional losses are also present, such as leakage losses, disk friction losses, and mechanical losses, but are not directly affecting the pump curve. The friction losses are usually written as $k_1 \cdot Q^2$, where k_1 is a constant that includes all unknown parameters. The impact losses are expressed as $k_2(Q - {}^*Q)^2$, which are present for all operational points outside the designed volume flow rate. When including the hydraulic losses, the expression of the actual head can be derived:

$$H = \frac{u_2}{g} \cdot \left(u_2 \cdot \gamma - \frac{Q}{\pi \cdot D_2 \cdot B_2 \cdot \tan\beta_{2\infty}} \right) - k_1 \cdot Q^2 - k_2 \cdot (Q - {}^*Q)^2 \quad [m] \quad (2.17)$$

The loss coefficients k_1 and k_2 are estimated by comparison of laboratory measurements. k_1 is found from the highest efficiency point on the pump characteristics where impact losses are assumed zero. k_2 is estimated from the head for zero flow [8].

2.3.4 Affinity laws

A centrifugal pump will normally operate at variable rotational speed. Therefore, one might desire to examine how the change of rotational speed effect the hydraulic efficiency. Assuming the streamlines to remain unchanged with variable rotational speed, the geometry of the velocity diagrams for inlet and outlet remains the same. With this assumption, and supposing constant efficiency, the *affinity laws* can be derived [3]:

$$\frac{Q_1}{Q_2} = \frac{n_1}{n_2} \quad (2.18)$$

$$\frac{H_1}{H_2} = \left(\frac{n_1}{n_2}\right)^2 \quad (2.19)$$

$$\frac{P_1}{P_2} = \left(\frac{n_1}{n_2}\right)^3 \quad (2.20)$$

For the above equations, the subscripts 1 and 2 represent two different rotational speeds. By including the pump characteristic curve for various rotational speeds, the efficiency can be specified as a contour map for a given rotational speed, as seen in Figure 2.4. The given parameters in the diagram are relative to the best operational conditions for the pump.

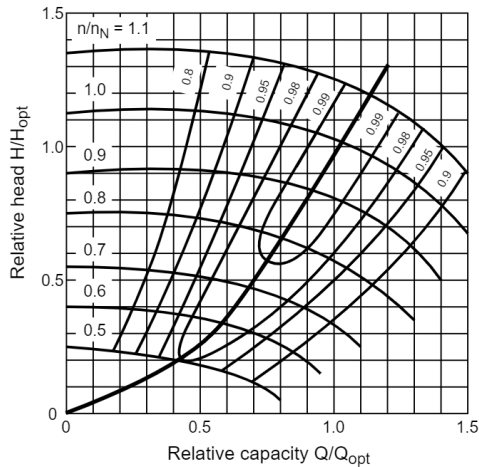


Figure 2.4: Regulation of rotational speed with efficiency curves [3].

2.4 Flow phenomena

This section introduces the flow phenomena cavitation and generation of pressure pulsation. To decide the magnitude of such phenomena is important, viewed from an economic perspective, as cavitation and pulsation cause fatigue fractions and erosion of pump components.

2.4.1 Cavitation

When the static pressure of a liquid decrease below the vapor pressure, the liquid will evaporate locally with formation of vapor cavities. This phenomenon is referred to as cavitation. The vapor pressure of the liquid depends on temperature and can be very low at atmospheric temperature. It is still possible to attain such low pressures at the suction side of the pump and is why cavitation is a phenomenon of importance as it has damaging consequences [7].

Consequences of cavitation

When vapor bubbles are transported downstream to zones where the static pressure again exceeds the vapor pressure, the bubbles rapidly collapse. This occurrence is termed implosion and generate intense pressure pulses. If the implosion occurs close to the confining structure, this can lead to erosion of the pump components. While cavitation can cause material fatigue, the bubbles can also affect the flow. During incipient cavitation, being the first formation of vapor bubbles, the performance data do not change. With significant vapor bubbles zones, termed developed cavitation, the flow is disrupted and results in higher losses. This sort of cavitation causes a decrease in both pump efficiency and head [7].

Cavitation assessment

The approach to decide the magnitude of cavitation is commonly referred to as the *Net Positive Suction Head (NPSH)*. As defined in Equation 2.21, $NPSH_A$ is the difference between the total pressure and the vapour pressure, and is the *available NPSH* at the suction side [7].

$$NPSH_A = \frac{p_s - p_v}{\rho \cdot g} + \frac{c_s^2}{2 \cdot g} \quad [m] \quad (2.21)$$

The total suction eye pressure and the vapor pressure are denoted p_s and p_v , respectively, and the velocity at the inlet is denoted c_s . To avoid cavitation, one must indicate a minimum positive value for $NPSH$. $NPSH_R$ is the required NPSH evaluated at the minimum suction pressure to avoid cavitation. Gülich [1] states numerous cavitation criteria, i.e., the permitted extent of cavitation. One such criterion is cavitation inception observed at $p_s = p_v$, where the formation of the

very first vapor bubbles appears. Because it is easy to measure, the most commonly used cavitation criterion is denoted as $NPSH_3$ and indicates a head drop of 3%. Several cavitation criteria are listed in Table 2.1.

Parameter	Description
$NPSH_i$	Visual cavitation inception
$NPSH_o$	Starting of head drop
$NPSH_1$	Head of suction impeller drops by 1%
$NPSH_3$	Head of suction impeller drops by 3%
$NPSH_{FC}$	Full cavitation, head of impeller is severely reduced

Table 2.1: Cavitation criteria [1].

2.4.2 Pressure pulsations

Pressure pulsations are fluctuations from the produced pressure in the pump. These pulsations can sometimes be severe and cause damage to the pipe system and other components in the hydraulic system. The pulsations are mainly caused by the phenomena described below.

Rotor-Stator Interaction: A pressure pulse is created each time a blade of the impeller passes the cutwater near the outlet and is termed Rotor-Stator Interaction (RSI). The position of the cutwater can be seen in Figure 2.5. When the blade tip is next to the cutwater, the maximum amount of energy caused by fluid motion is directed against the pump outlet. After passing this point, some water will flow through the space between the cutwater and the impeller, causing a drop of discharge energy. The change of minimum and maximum energy transfer results in a corresponding change in the outlet pressure, generating pressure pulsations. The distance between the cutwater and the impeller decides the magnitude of the pulsations, and the frequencies from RSI will manifest in the spectrum as rather sharp, discrete peaks [9].

Von Karman vortex shedding: A second contribution to pressure pulsations are the formation of repeating patterns of swirling vortices caused by alternating flow separation. These vortex streets form downstream of the impeller blade, i.e., the trailing edge. This phenomenon is called von Karman vortex shedding and creates pulsations with the same frequency as the formation of swirling components [1].

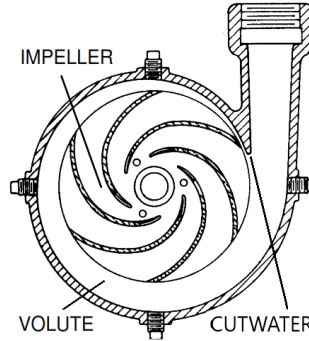


Figure 2.5: Cutwater in the volute casing.

Frequencies

Pressure pulsations can be explained with quantities in terms of frequency and amplitude. A frequency is the number of periodic occurrences in a unit of time. The RSI is dependent on the number of times a blade passes the cutwater and is defined by Equation 2.22 [1]

$$f_{RSI} = N \cdot \frac{n}{60} \quad [Hz] \quad (2.22)$$

where N denotes the number of impeller blades, and n indicates the rotational speed of the impeller. The frequency from the von Karman vortex shedding for general geometries is determined with Equation 2.23 [10].

$$f_v = St \cdot \frac{B}{100} \cdot \frac{U}{t + \delta_v} \quad [Hz] \quad (2.23)$$

B denotes the constant geometry shape factor and St the Strouhal number calculated based on the Reynolds number. U represent the flow velocity and the term $(t + \delta_v)$ is the blade thickness added to the boundary layer thickness. The boundary layer thickness is found using Equation 2.24

$$\delta_v = 0.0293 \cdot \frac{x}{Re_x^{1/5}} \quad [m] \quad (2.24)$$

where x denotes the blade length and Re_x is the Reynolds number at x .

Analysing pressure pulsations

To examine the pressure pulsations one must perform a frequency analysis. The recorded data can be extracted from the time-domain and transformed into the frequency-domain. This results in a frequency spectrum containing discrete peaks that represents the pressure pulsations. One common analysis is the Discrete Fourier Transformation which is based on Fast Fourier Transformation. The analysis allows the periodic non-harmonic signals to be described as a sum of sinusoidal partial components[1].

When logging the data, it is important to use a sufficiently high sampling rate in order to obtain a continuous representation of the discrete data points. The Nyquist frequency defines the upper frequency as $f_{Ny} = f_s/2$ where f_s is the sampling rate. If the sampling rate is too low, spectral lines above f_{Ny} can fold back below this domain and is referred to as aliasing. Gülich [1] defines a sufficient limit for the sampling rate with Equation 2.25, where f_{max} is the maximum expected frequency to be found.

$$f_s = (2.2 - 3) \cdot f_{max} \quad [Hz] \quad (2.25)$$

2.5 Uncertainty in experiments

Measurements of a physical quantity include some degree of uncertainty arising from distinct errors. An error represents the difference between the measured and true value of the quantity. The uncertainty in the measurement is the range where the true value can be expected to lie. With statistical methods, one can find a confidence interval where the true value of the measured quantity will lie within, with a specified probability [11]. The IEC 60193 standard state a 95 % probability of the confidence interval and is the confidence interval used for these experiments [12].

2.5.1 Spurious errors

Spurious errors arise from human errors, or instrument malfunction, which makes the measurement invalid. These errors should not be included in the statistical analysis and should be discarded [11].

2.5.2 Random errors

Random errors are caused by numerous, small, independent influences leading to different readings from the measurement system when the input value is the same for the measured quantity. This causes a deviation from the mean value, and one can assume that the recorded data approaches a *Normal distribution* as the number of measurements increases. This assumption indicates that the random error will

decrease with an increasing number of measurements. If the sample size is lower, the distribution is described using a *Student-t distribution* [11].

The confidence interval for the mean of the measurement, \bar{Y} , in a Student-t distribution is defined in Equation 2.26.

$$\bar{Y} \pm \frac{t \cdot S_Y}{\sqrt{n}} \quad (2.26)$$

$$S_Y = \sqrt{\frac{1}{n-1} \sum_{i=1}^n (Y_i - \bar{Y})^2} \quad (2.27)$$

where n denotes the number of recorded points in the measurement, t represent the tabulated t-value according to the degree of freedom ($n - 1$), and S_Y denotes the standard deviation. The real mean value for a sequence of recordings with a 95 %-confidence level will be within the confidence interval described in Equation 2.26 with a probability of 95 %.

2.5.3 Systematic errors

Systematic errors have the same magnitude during the same conditions of measurement. If the equipment and conditions for the measurements remain the same, the error does not decrease by increasing the number of measurements. In some cases, the equipment has a unique known value and should be added to the measured result. If the systematic error of the equipment is unknown, but the error limits are specified, the interval between them may be assumed as the uncertainty, with a confidence interval of 95 % [12].

2.5.4 Regression error

The calibration curve results in a linear approximation line to best fit the scattered data points. The random variation around the regression line can be described with the following equations:

$$S_{XX} = \sum_{i=1}^n (x_i - \bar{X})^2 \quad (2.28)$$

$$S_{YY} = \sum_{i=1}^n (y_i - \bar{Y})^2 \quad (2.29)$$

$$S_{XY} = \sum_{i=1}^n (x_i - \bar{X})(y_i - \bar{Y}) \quad (2.30)$$

While S_{XX} and S_{YY} describes the variation of x and y individually around the regression line, S_{XY} describes the combined variation of x and y about the linear line. The *sum squares error* (SSE) for the regression line can be written as shown in Equation 2.31. SSE can be applied to express the unbiased estimate of the variance of the regression line as in Equation 2.32 [13].

$$SSE = S_{YY} - \frac{S_{XY}^2}{S_{XX}} \quad (2.31)$$

$$s^2 = \frac{SSE}{n - 1} \quad (2.32)$$

The absolute uncertainty for some value Y_0 of an input x_0 is defined by Equation 2.33. $e_{Y|x_0}$ should be calculated for the whole linear regression line, by using each corresponding x-value [11].

$$e_{Y|x_0} = \pm t_{\alpha/2} \cdot s \sqrt{\frac{1}{n} + \frac{(x_0 - \bar{X})^2}{S_{xx}}} \quad (2.33)$$

Chapter III

Test rig setup

The test rig is installed at the Waterpower Laboratory at NTNU, which has numerous possible configurations and test conditions. In order to understand the rig setup and the pipe system, a brief description of the Waterpower Laboratory is given, followed by a description of the test rig for the centrifugal pump and the instrumentation installed for the measurements.

3.1 Waterpower Laboratory

Presented in this section is the components installed in the Waterpower Laboratory that the test rig utilizes during operation. The laboratory is built around a complex pipe system and has the opportunity of different running conditions by using different pipe systems. The test rig for the centrifugal pump configures an own pipe system, connected to the pressure tank and the feed pumps in the basement, supplied with water from the lower reservoir.

3.1.1 Lower water reservoir

The main water reservoir is located under the laboratory floor and has a capacity of 450 m^3 . The water in the lower reservoir, or commonly referred to as the sump, is cleaned or changed regularly to assure a sufficient water quality [4].

3.1.2 Feed pumps

The laboratory is implemented with two main feed pumps in the basement, located 4.775 m below the laboratory floor. The pumps are of the RDLO type series and are produced by KSB. They are horizontally installed, single-stage, axially split volutes casing pumps. Both pumps are controlled automatically from the control room located in the laboratory. The pumps can be run individually or connected in series or parallel, depending on whether high pressure or high volume flow is

required [4].

3.1.3 Loop configurations

Because of the complex pipe system in the laboratory it is possible to run tests for different conditions and configurations. A u-shaped, free surface channel is located on the 5th floor of the building, which enables to run tests in open loop configurations with a constant head of approximately 16 m. For configurations with larger head, the water circuit runs in a closed loop through the pressure tank [4]. Both loops are illustrated in figure 3.1.

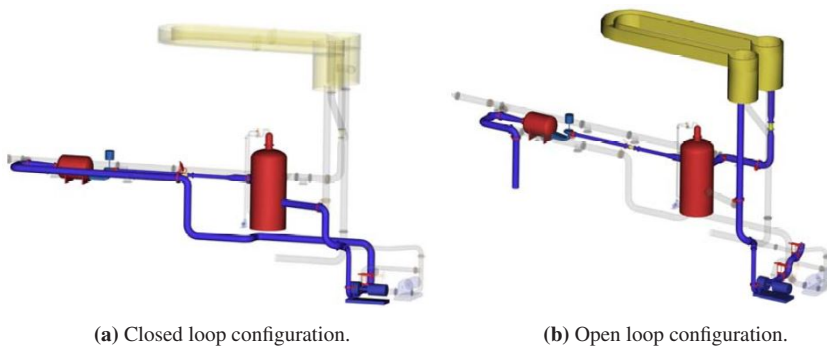


Figure 3.1: Loop configurations in the Waterpower Laboratory [4].

3.1.4 Pressure tank

In the laboratory, a pressure tank is installed vertically and has a volume of 15 m³ for 10 bar pressure at 20 °C. The tank can be utilized to produce the head for all loop configurations in the laboratory [4]. Shown in figure 3.1, is the pressure tank in red beneath the yellow u-shaped, free storage reservoir.

3.2 Rig design

This section describes the centrifugal pump test rig and its components. The rig was designed in SW during the authors project thesis in the fall semester of 2019. A decent amount of time have been spent in the laboratory setting up the rig based on this design.

3.2.1 Base design

The rig was designed based on an initial rig in the Waterpower Laboratory, as shown in Figure 3.2. Located in the back part of the red frame is an electrical engine produced by Siemens. The control unit for the engine power output is manual and is adjusted according to the desired rotational speed. The engine shaft goes from the engine, through the torque transducer, where the torque is measured and further into the bearing block meant to support the rotating shaft.

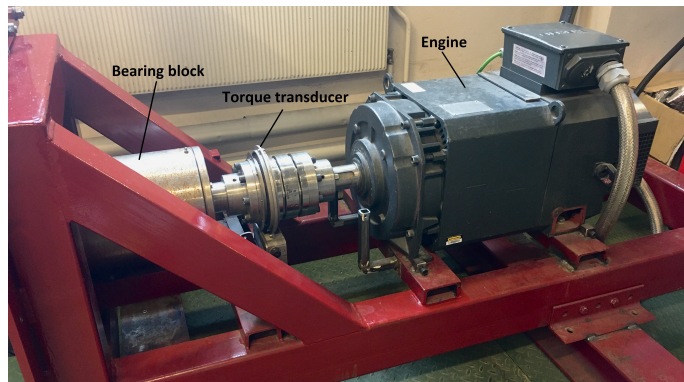


Figure 3.2: Initial rig setup.

3.2.2 Belt drive

As the installed engine could not provide a sufficient output power to reach the designed rotational speed, the solution was to install a gearing belt drive system. Such a system can gear up speeds by power transmission between a small and a larger gear drive using a rubber timing belt. Also, it was installed a belt tensioner to reduce the slip. With the described belt drive system, the rotational speed of the pump shaft was increased by a ratio of 8. Figure 3.3 shows the belt, gear drives, and tensioner installed in the rig.

3.2.3 Brackets

It was manufactured two types of brackets, used to install the pump in a secure position. To ensure correct alignment between the pump and the gear drive, two horizontally mounted brackets close to the pump shaft were installed. Four other brackets were installed between the side of the volute and the backside plate, to assure further stabilization. The bracket installation can be seen in Figure 3.3.

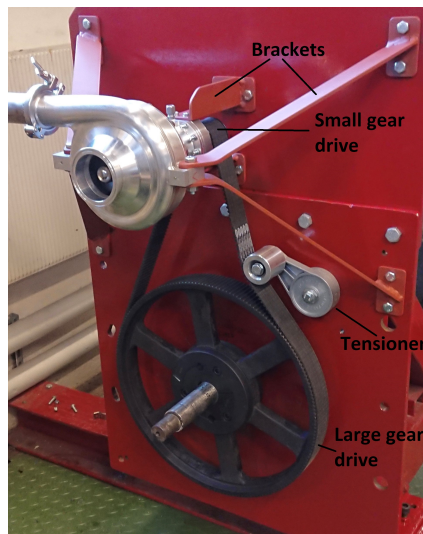


Figure 3.3: Installation of belt drive system and brackets.

3.2.4 V- clamps

V-clamps were used to connect the flange on the inlet and outlet pipes to the suction eye and discharge side on the pump. At the intersection of the flanges, a seal was locked between the clamps to assure no leakage.

3.2.5 Setup for cooling

The pump is equipped with two ball bearings close to the impeller. The pump casing is designed with a flush port to assure cooling of the bearings. The flush port was connected, through a plastic tube, to a small 3 mm tap on the inlet pipe, as seen in Figure 3.5(a). With this configuration, the water could flow into the flush port, shown in Figure 3.5(b), and through the ball bearings.

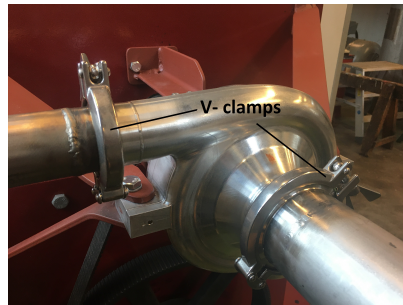
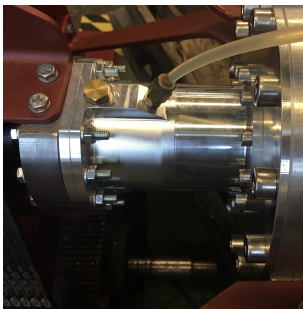
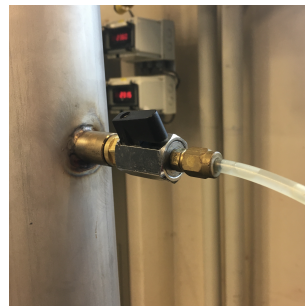


Figure 3.4: V-clamps at the inlet and outlet.



(a) Flush port on pump for cooling. Tap on inlet pipe



(b) Tap on inlet pipe.

Figure 3.5: Setup for cooling of bearings.

3.2.6 Valve

Installed at the vertical part of the outlet pipe was a manual valve used to regulate the flow rate. Because the water goes down from the discharge nozzle to the lower water reservoir with a free atmospheric surface, this installation was also necessary to assure sufficient resistance for the outlet pressure.

3.3 Instrumentation

This section presents the instrumentation installed in the test rig that was applied to conduct the measurements. The instrumentation at the Waterpower Laboratory is approved certified by the IEC 60193 standard [12], and the instrumentation is installed accordingly. The instrumentation for the rig includes a torque transducer, flow meter, rotational speed counter, and pressure transducers. The instruments were connected to a computer through a National Instruments logging card, and the computer was equipped with a specialized software created in LabView for recording measured data.

3.3.1 Pressure

The pressure was measured using two GE Druck absolute pressure transducers, one at the inlet with a range of 0–6 *bar* and one at the outlet ranging from 0–30 *bar*. The transducers give an output signal ranging from 4–20 *mA*, which is converted into a voltage signal ranging from 2–10 *V*. The installation of the GE Druck absolute pressure transducer can be seen in figure Figure 3.6. The pressure transducers were connected to taps on the inlet and outlet pipes of the rig.

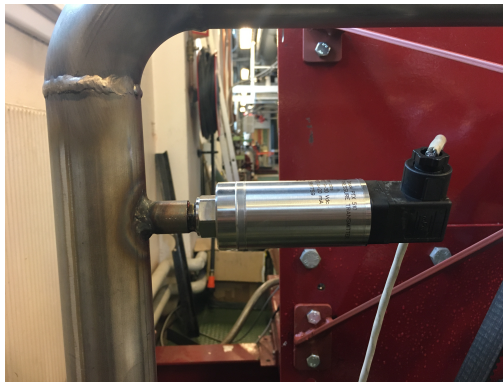


Figure 3.6: Installation of pressure transducer on the outlet pipe.

3.3.2 Volume flow rate

An electromagnetic flow meter was used to measure the volume flow rate. The water is a conductive fluid and flows in a non-conductive pipe with a magnetic field and electrodes. The magnitude of the voltage induced between the electrodes is proportional to the speed of the moving fluid [2].

The flow meter installed was an Optiflux 2300C Ø100 electromagnetic flow meter

manufactured by Krohne, with a range of 0–70 l/s . An IFC 300 signal converter was connected to the flow meter. The instrument reads the induced voltage and calculates the flow rate, with an output signal in mA . Figure 3.7 shows the flow meter installed with the signal converter. The flow meter was installed according to the IEC 60193 standard [12], avoiding bends and junction of the pipe.



Figure 3.7: Optiflux 2300C with an IFC 300 signal converter.

3.3.3 Torque

The torque provided on the engine shaft was measured using a T10F torque transducer produced by HBM and can be seen in Figure 3.8(a). The torque transducers use strain gauges applied to the rotating engine shaft and gives an output signal in mA before it is converted into a volt signal.

The torque transducer is mounted to the shaft between the engine and the bearing block in the rig. Ideally, the torque should be measured at the impeller shaft because of the mechanical losses that occur in the driving belt system. Due to economic limitations, it was decided not to procure a new torque transducer that was possible to install the impeller shaft, and instead account for the mechanical losses through the power transmission. The mechanical efficiency through the belt drive system was given by the producer to be approximately 95%.

3.3.4 Rotational speed

The rotational speed was measured with a piece of reflective tape attached to the rotating shaft, an infrared light source, and an optical rotation counter. For each time the reflective tape passes the infrared light beam, the light is reflected back to the optical rotation counter, and the numbers of rotations per minute are found. A piece of reflective tape was also attached to the pump shaft to verify the geared rotational speed through the belt drive to be correct. The setup of the rotational speed measurement can be seen in Figure 3.8(b) and was installed next to the torque meter.

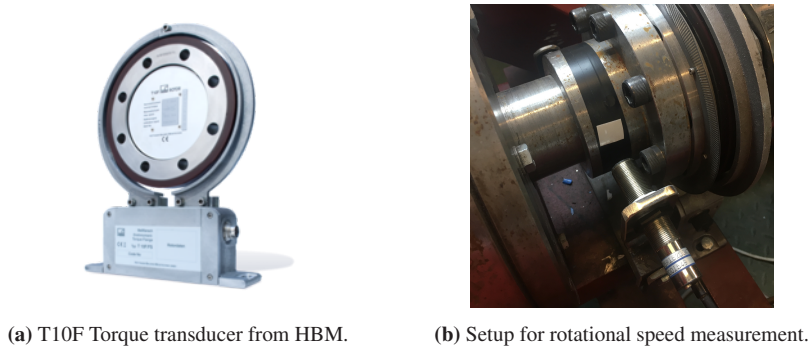


Figure 3.8: Torque transducer and rotational speed instrumentation.

3.4 Rig setup in the laboratory

Figure 3.9 shows a schematic of the rig in the laboratory facility and the installed instrumentation. The water is fed to the pressure tank by the feed pump in the basement to obtain a constant inlet pressure for the centrifugal pump. Further, the water leaves the pressure tank, and the volume flow rate is measured by the electromagnetic flow meter. After the valve, the static pressure is measured by an absolute pressure transducer, ranging from 0–6 *bar*, before entering the suction eye of the centrifugal pump. The second pressure transducer is mounted at the outlet pipe, ranging from 0–30 *bar*, measuring the static pressure of the flow after leaving the pump outlet. Before going back into the lower water reservoir, the water passes the manual valve for regulating the flow rate. A procedure on how to operate the test rig for the centrifugal pump is described in detail in Appendix D.

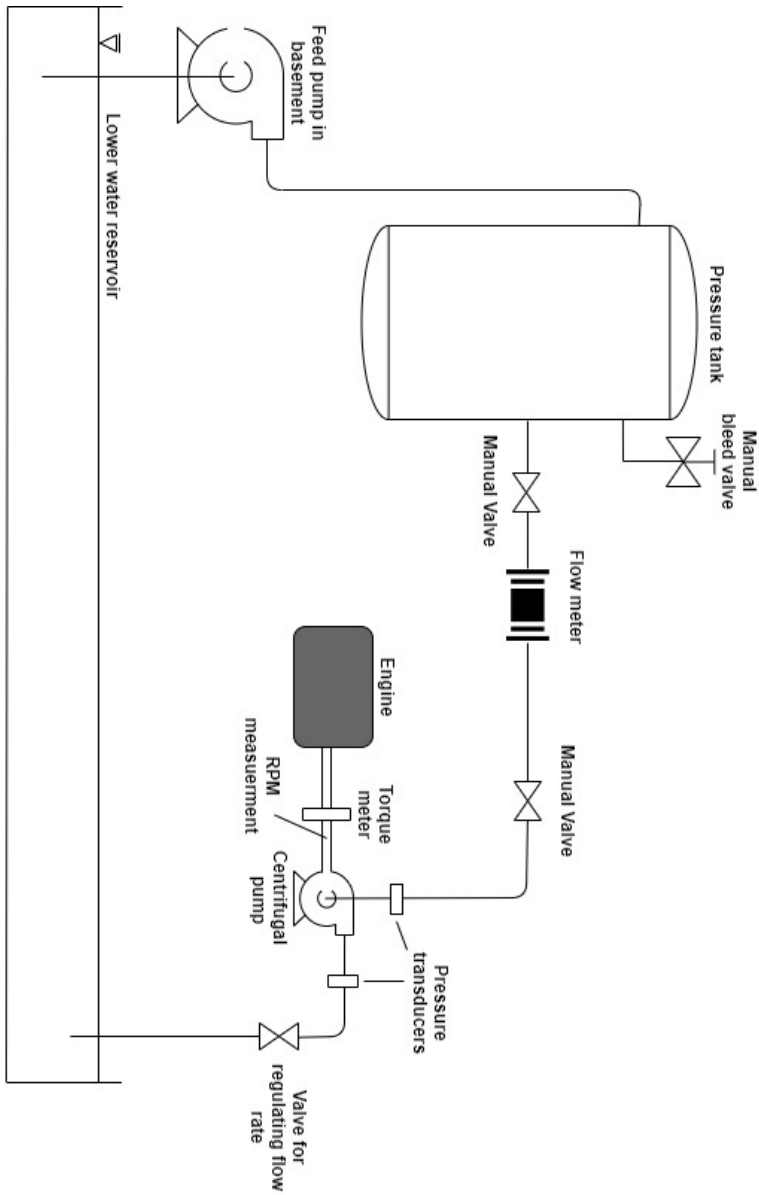


Figure 3.9: Schematic of the rig setup in the Waterpower Laboratory.

Chapter IV

Experimental methods and calibration

This chapter presents the work conducted in the laboratory related to this thesis. First introduced is the calibration procedure done for each instrument, followed by description of the experimental methods applied in this study. The chapter also includes the procedure of 3D printing that was performed to create a model of the impeller.

4.1 Calibration

This section describes the calibration procedures performed on the instrumentation presented in chapter 3. Each procedure includes the obtained regression line found after the calibration, along with its total error band. All the calibration procedures are elaborated in Appendix A.

4.1.1 Linear regression

Calibration is done to ensure a correct relation between sensor output, i.e., V or mA , and the physical value measured. The results from the calibration are applied to convert the test data in order to obtain more accurate results [14]. Calibration must be performed using primary methods based on quantities such as length, time, and mass. Devices using secondary methods of measurements must be calibrated against a primary method [2].

The measured points from the calibration create a linear regression line. Because the uncertainty is higher in the beginning and the end of the curve, several calibration points must be obtained in these areas. The correct parameter in question can be calculated with the following linear regression equation:

$$y = a \cdot MV + b \quad (4.1)$$

where y denotes the value being calculated, MV is the measured value and a and

b are the calibration constants [14].

Since the measured property for rotational speed is time, this is a primary method and calibration is not required. Pressure, flow rate, torque, and temperature is measured by secondary methods and the calibration procedures are described in the following sections.

4.1.2 Calibration of the pressure transducers

The pressure transducers were calibrated with a dead weight manometer, defined as a primary method by the IEC 60193 standard [12]. The manometer is produced by GE Sensing of the type P3223-1.

Several calibrated weights with indicated pressure were loaded onto a cylindrical disk mounted on top of a piston. The mass of the weights and the gravitation produced a force acting on the known area of the piston cylinder. The piston pressurized the fluid with known density ρ , in the chamber with a pressure indicated by Equation 4.2.

$$p_{manometer} = \frac{F}{A_{piston}} = \frac{m \cdot g}{A_{piston}} \quad [Pa] \quad (4.2)$$

Here, F denotes the force acting on the known area A_{piston} , m denotes the total mass for each load and g denotes the gravitational constant.

Both transducers were positioned $Z_{cal} = 0.082m$ above the zero point of the manometer. Equation 4.3 was used to calculate the total pressure measured by the transducers.

$$p_{total} = p_{manometer} - \rho \cdot g \cdot Z_{cal} \quad [Pa] \quad (4.3)$$

Figure 4.1 and Figure 4.2 shows the calibration curve for the inlet and outlet pressure transducers, respectively, with a total error band and a confidence level of 95% for the regression error.

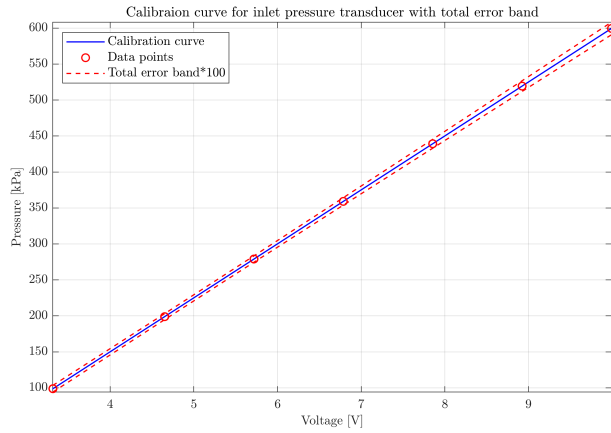


Figure 4.1: Calibration curve for the inlet pressure transducer with a total error band scaled by 100.

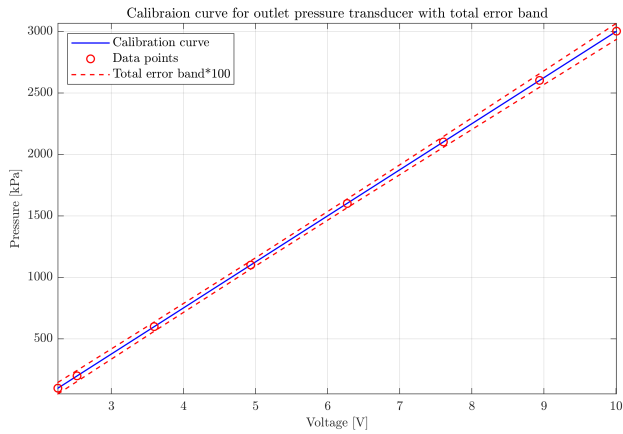


Figure 4.2: Calibration curve for the outlet pressure transducer with a total error band scaled by 100.

4.1.3 Calibration of the flow meter

The flow meter was calibrated using the weighing method, recommended as a primary method by the IEC 60193 standard [12]. The calibration was conducted using the weighing tank system located in the Waterpower Laboratory. The weighing tank is equipped with three load cells of the type Hottinger RTNC, connected to an amplifier, and several calibrated weights on top of the tank. The weight displayed on the amplifier must be corrected, so a substitution calibration was performed to find the correction equation for the weights [4]. Equation 4.4 shows the fifth-order polynomial correction equation for the weight.

$$W = a_0 \cdot \frac{c^5}{5} + a_1 \cdot \frac{c^4}{4} + a_2 \cdot \frac{c^3}{3} + a_3 \cdot \frac{c^2}{2} + a_4 \cdot c \quad [kg] \quad (4.4)$$

After calibrating the weighing tank, the electromagnetic flow meter was calibrated. The flow was adjusted with a manual valve located right before the inlet of the weighing tank. By measuring the weight before and after, and the time during filling, the mean flow rate was calculated using Equation 4.5. The weight before and after filling, W_1 and W_2 , was corrected using Equation 4.4. The water and air density were corrected with equations found in Appendix A.2.

$$Q = \frac{W_2 - W_1}{\rho_w \cdot t \cdot \left(1 - \frac{\rho_{amb}}{\rho_w}\right)} \quad [m^3/s] \quad (4.5)$$

The result of the substitution calibration of the weighing tank and the flow meter can be seen in Figure 4.4 and Figure 4.3, respectively.

During calibration, one should measure several data series, going up and down between minimum and maximum values of the flow rate. During this procedure, the measurements should be done at the same data points. As the valve for adjusting the flow is manual and sensitive, difficulties occurred when trying to measure at the same data point. As seen in Figure 4.3, the measured data points are more scattered, and this affects the regression error for the calibration curve, further discussed in chapter 5.

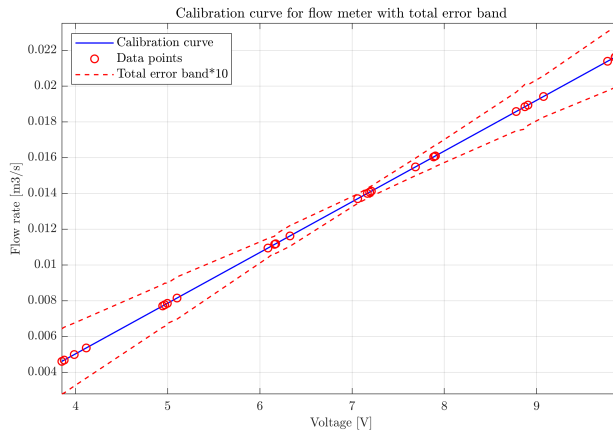


Figure 4.3: Calibration curve for the electromagnetic flow meter with a total error band scaled by 10.

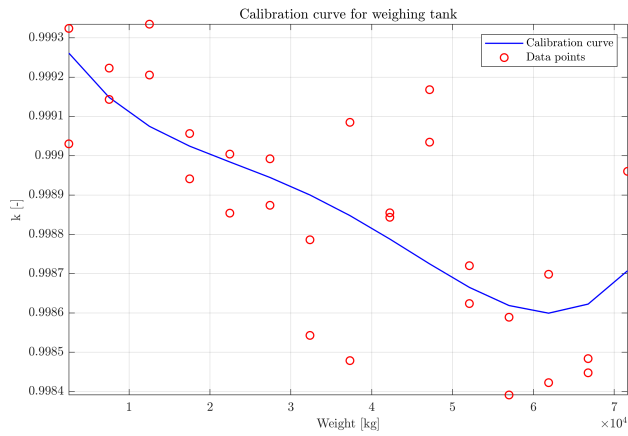


Figure 4.4: Calibration curve for the weighing tank.

4.1.4 Calibration of the torque transducer

The torque meter was calibrated by applying a torque to the engine shaft using multiple calibrated weights and is recommended as a primary method by the IEC 60193 standard[12].

The engine shaft was fixed to avoid rotation, and a lever arm was mounted onto the shaft in a centered position. The arm was then balanced and gave no contribution to the torque. A fixture was attached to the arm, at a known length L from the shaft. A number of calibrated 5 kg weights were loaded onto the fixture creating a force perpendicular to the arm.

$$T = F \cdot L = m \cdot g \cdot L \quad [Nm] \quad (4.6)$$

The torque was calculated with Equation 4.6, where $L = 0.5\text{m}$ denotes the known length of the arm, g is the gravitational constant, and m denotes the total mass of the fixture and the weights loaded. Figure 4.5 shows the resulting calibration error curve for the torque transducer with a 95 % confidence interval for the regression error.

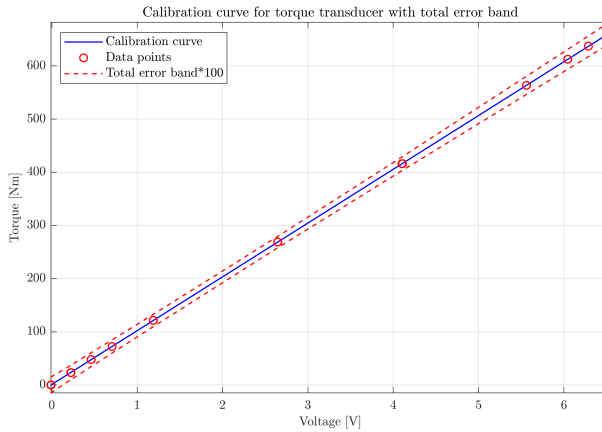


Figure 4.5: Calibration curve for the torque transducer with a total error band scaled by 100.

4.2 Experimental method

The main objective of this thesis was to perform hydraulic efficiency measurements and examine the pump characteristics, presented in an HQ-curve. This section will describe how the tests were conducted to obtain the pump characteristics for the centrifugal pump.

4.2.1 Test procedure

The rotational speed, inlet and outlet pressure, volume flow rate, and torque was measured and logged using a general logging program in LabView. In order to obtain one curve for the pump characteristics, the pump was set to a constant rotational speed and constant inlet pressure. The first data point was measured with maximum flow. After recording the first data point, the manual valve was closed with small increments for each new data point. By repeating this step until the minimum possible flow rate, the range for the HQ-curve was obtained. A more detailed test procedure may be found in Appendix D, along with procedures for starting and shutting down the rig.

4.2.2 Post-processing

The post-processing of the data obtained from the measurements was done in MatLab. The measured data was imported in MatLab and converted to a .mat-file using a general file converter. Given below is a description for each code applied to sort and calculate the data. T Appendix F contains the codes used in this thesis.

DataSort.m Reads the .mat-file, creates a matrix of the mean values from the raw data and calculates the measured quantities based on the calibration constants. The script further calculates H , P_h, P_m and η_h . The matrix is saved as a .xlsx-file.

HQcurve.m Reads the .xlsx-file and plots the HQ-curve, with and without affinity laws and the efficiency curve as a function of Q .

4.2.3 Correction of outlet pressure

A difficulty during testing was to achieve a sufficient pressure increase between the inlet and outlet. After adjusting the valve, the outlet pressure was lower than the inlet pressure for high flow rates. As the static pressure has a large impact on the head, this resulted in negative values of the head during the first measured data points. It was assumed that the cause for the low outlet pressure was the

installed outlet pressure transducer, as it was located a short distance downstream a bend on the pipe. The flow normally experiences a pressure drop when going through bends. The magnitude of the corrected outlet pressure was estimated using an approximation for pressure drop in 90° bends, shown in Equation 4.7 [15].

$$\Delta p_{bend} = \frac{1}{2} \cdot f \cdot \rho \cdot U^2 \cdot \frac{\pi \cdot R_b}{D} \cdot \frac{90^\circ}{180^\circ} + \frac{1}{2} \cdot k_b \cdot \rho \cdot U^2 \quad [Pa] \quad (4.7)$$

The bend loss coefficient, $k_b = 0.34$, was found based on the ratio between the bend radius, R_b , and the internal pipe diameter, D , found to be 1.4. f denotes the friction factor, and U denotes the mean velocity.

4.2.4 Rapid prototyping

During the manufacturing process, the impeller was damaged and had the potential to cause a significant delay in the laboratory work. As an alternative option, 3D-printing was investigated using an Original Prusa i3 MK3 3D printer.

Procedure for 3D-printing

The CAD drawing of the impeller was saved as an stereolithography (STL) file from SW. The STL-file defines the surface geometry of the part by using unstructured triangles. Further, the file was imported to PrusaSlicer. As the impeller had a complex geometry with overhang and curves, it was necessary to build a support structure for the surfaces. After completing the construction in PrusaSlicer, the file was exported as a G-code and saved to the printer's memory card. Appendix E gives a step-by-step procedure on how to create a 3D-print.

Filament

The impeller was printed using both PLA and water-soluble filament. The impeller was printed using the PLA, while the soluble filament was used at the interface between the impeller surface and the support structure. Usually, the support structure made with PLA is hard to remove without leaving a high surface roughness. As the impeller surface must be smooth to lower the impact of friction losses, the soluble filament at the interface was the right solution. After finishing a print, the part is put in water until the soluble filament is dissolved and gives a smoother surface.

Chapter V

Uncertainty analysis

This chapter presents the significant random and systematic errors detected during both the calibration and measurement procedures. The significant errors from each procedure are tabulated and are used to calculate the total uncertainty of the efficiency. The magnitude of the uncertainties presented in this chapter counts for the highest measured hydraulic efficiency found from testing, which was 42.29 %.

5.1 Uncertainty in calibration

An error can be expressed both as absolute and relative. The absolute error of some quantity X is denoted e_X and is expressed in the units of the measured quantity. The relative error is defined as $f_X = e_X/X$. There are various error components in the calibration procedure, both random and systematic, for the primary and secondary instruments. Table 5.1 shows the components of the relative error for some quantity X , which counts for all calibration procedures and are defined by the IEC 60193 standard [12].

Error	Description
$\pm f_{X_a}$	Systematic error of the primary calibration instrument
$\pm f_{X_b}$	Random error of the primary calibration instrument
$\pm f_{X_c}$	Systematic error of the secondary calibration instrument
$\pm f_{X_d}$	Random error of the secondary calibration instrument
$\pm f_{X_e}$	Physical phenomena and influence quantities
$\pm f_{X_f}$	Errors in physical properties

Table 5.1: Error components in the calibration procedure.

All components listed in Table 5.1 contributes to the total uncertainty in the calibration curve, denoted $f_{X_{cal}}$. The *Root-sum-square* (RSS) method is used to calculate

the total uncertainty and is shown in Equation 5.1.

$$f_{X_{cal}} = \pm \sqrt{(f_{X_a})^2 + (f_{X_b})^2 + (f_{X_c})^2 + (f_{X_d})^2 + (f_{X_e})^2 + (f_{X_f})^2} \quad (5.1)$$

5.1.1 Uncertainty in the calibration of pressure transducers

The total uncertainty of the dead weight manometer is denoted as $f_{p_{ab}}$ being the sum of the relative systematic and random error of the calibration instrument. According to the documentation following the dead weight manometer, the total error in the instrument does not exceed $\pm 0.008\%$. The error is found by combining f_{p_a} and f_{p_b} with the RSS-method.

f_{p_c} is the systematic error in the secondary instrument, which in this case, is the pressure transducers. Calibration is done to minimize this uncertainty by calibrating the instrument signal against a physical quantity, here being the dead weight manometer. During calibration, one cannot calibrate for all possible pressures. This produces a systematic uncertainty and is denoted $f_{p_{regression}}$. The random error in the instrument, f_{p_d} , is caused by scattering of the signal while logging over time. This uncertainty is also included in $f_{p_{regression}}$. The error due to physical phenomena and external influences for the pressure transducer calibration is denoted f_{p_e} and is assumed to be negligible in this case [11].

f_{p_f} is the error in the physical properties from calculation or the usage of international standard data. This uncertainty includes the uncertainty of the measurement of the height difference Z_{cal} between the zero point of the dead weight manometer and the measuring point for the pressure transducer. Z_{cal} was measured with a sliding gauge, and the uncertainty of this device was assumed to be 0.0001 m. As the height difference was $Z_{cal} = 0.02724m$, the relative uncertainty was found with $f_{p_{i_f}} = \frac{Z_{cal} \cdot \rho \cdot g}{p_i}$. Table 5.2 lists all the uncertainties contributing to the total relative uncertainty from the pressure transducer calibration, and counts for the measured inlet and outlet pressure measured to be 3.9 bar and 4.84 bar, respectively.

The total relative uncertainty of the calibration of the inlet and outlet pressure transducers was calculated with Equation 5.2 and Equation 5.3, respectively.

$$f_{p1_{cal}} = \pm \sqrt{(f_{ab})^2 + (f_{p1_{regression}})^2 + (f_{p1_f})^2} = \pm 0.0142\% \quad (5.2)$$

$$f_{p2_{cal}} = \pm \sqrt{(f_{ab})^2 + (f_{p2_{regression}})^2 + (f_{p2_f})^2} = \pm 0.0634\% \quad (5.3)$$

Uncertainty	Description	Magnitude
$f_{p_{ab}}$	Total error of the dead weight manometer	$\pm 0.008\%$
$f_{p1_{regression}}$	Systematic and random error in the inlet transducer	$\pm 0.0117\%$
$f_{p2_{regression}}$	Systematic and random error in the outlet transducer	$\pm 0.0629\%$
f_{p1_f}	Error in height difference Z_{cal} based on p_1	$\pm 0.0002\%$
f_{p1_f}	Error in height difference Z_{cal} based on p_2	$\pm 0.00017\%$

Table 5.2: Uncertainty in the calibration of the pressure transducer.

5.1.2 Uncertainty in the calibration of flow meter

The primary method used to calibrate the flow meter was the weighing tank system in the Waterpower Laboratory. f_{Q_a} and f_{Q_b} , listed in Table 5.3, are the relative systematic and random errors, respectively, contributing to the uncertainty of the primary instrument. Appendix C gives a more detailed calculation of the uncertainties for the flow meter calibration. The uncertainties was calculated for the measured flow rate at 10.4 l/s.

Uncertainty	Description	Magnitude
f_{Q_a}	Systematic error in the weighing tank	$\pm 0.0889\%$
f_{Q_b}	Random error in the weighing tank	$\pm 0.0503\%$
$f_{Q_{regression}}$	Systematic and random error in the flow meter	$\pm 0.5826\%$

Table 5.3: Uncertainty in the calibration of the flow meter.

The total uncertainty in the calibration of the flow meter was found by combining the listed values in Table 5.3 and with the RSS-method as seen in Equation 5.4.

$$f_{Q_{cal}} = \pm \sqrt{(f_{Q_a})^2 + (f_{Q_b})^2 + (f_{Q_{regression}})^2} = \pm 0.5915\% \quad (5.4)$$

5.1.3 Uncertainty in the calibration of torque transducer

The significant errors for the torque transducer calibration were the systematic error in the weights and the fixture, f_{T_W} , the systematic error in the length of the arm, $f_{T_{arm}}$, and the systematic and random error in the torque meter, included in $f_{T_{regression}}$. The random error of the primary method was neglected as neither the arm nor the weights have a random component related to their quantities. The uncertainties are calculated in Appendix C, for the torque measured at 77.75 Nm.

Uncertainty	Description	Magnitude
$f_{T_{arm}}$	Systematic error in the length of the arm	$\pm 0.02\%$
f_{T_W}	Systematic error in the weight of weights and fixture	$\pm 0.011\%$
$f_{T_{regression}}$	Systematic and random error in the torque meter	$\pm 0.156\%$

Table 5.4: Uncertainty in the calibration of the torque transducer.

Combining the uncertainties listed in Table 5.4 with the RSS-method, the total relative uncertainty in the calibration of the torque transducer was calculated using Equation 5.5.

$$f_{T_{cal}} = \pm \sqrt{(f_{T_{arm}})^2 + (f_{T_W})^2 + (f_{T_{regression}})^2} = \pm 0.1574\% \quad (5.5)$$

5.2 Uncertainty in the measurements

Table 5.5 refers to the errors present in the measurements, where X is the measured quantity. The uncertainty from the calibration, $f_{X_{cal}}$, covers both the systematic and random errors of the instrument, but the error becomes entirely systematic when the calibration error is included in the tests. The errors due to physical phenomena and influence quantities, f_{X_k} , may be neglected if the conditions for the calibration are constant during the tests. If not, f_{X_k} is both a systematic error, denoted $f_{X_{ks}}$, and a random error, denoted $f_{X_{kr}}$ [12].

Error	Description
$\pm f_{Xcal}$	Total uncertainty in the calibration
$\pm f_{Xh}$	Systematic error of the secondary instrument
$\pm f_{Xj}$	Errors in physical properties
$\pm f_{Xk}$	Physical phenomena and influence quantities
$\pm f_{Xl}$	Random error of the secondary instrument (repeatability)

Table 5.5: Error components from tests.

The systematic and random errors is calculated using Equation 5.6 and Equation 5.7. The total uncertainty is then found with Equation 5.8 [12].

$$f_{Xs} = \pm\sqrt{(f_{Xcal})^2 + (f_{Xh})^2 + (f_{Xj})^2 + (f_{Xks})^2} \quad (5.6)$$

$$f_{Xr} = \pm\sqrt{(f_{Xkr})^2 + (f_{Xl})^2} \quad (5.7)$$

$$f_{Xt} = \pm\sqrt{(f_{Xs})^2 + (f_{Xr})^2} \quad (5.8)$$

5.2.1 Uncertainty in the pressure measurements

The uncertainties in the pressure measurements contain the total uncertainty found from the calibration of the transducer, $f_{p_{cal}}$, and the random error in the measurement, f_{pl} . The random error in the measurement was found using the student-t confidence interval for the measured data.

The uncertainty caused by drifting of the output signal, f_{pn} , may be reduced by calibrating the instrument after the testing. Due to lack of time, this was not done, but the uncertainty is assumed to be ignored. Additional uncertainties such as f_{pk} and f_{pl} are also assumed to be negligible [11].

The total uncertainty in the pressure measurements for the inlet and outlet pressure transducer, are calculated with Equation 5.9 and Equation 5.10, respectively.

$$f_{p1} = \pm\sqrt{(f_{p1_{cal}})^2 + (f_{pl})^2} = \pm 0.0142\% \quad (5.9)$$

$$f_{p2} = \pm\sqrt{(f_{p2_{cal}})^2 + (f_{pl})^2} = \pm 0.0634\% \quad (5.10)$$

Uncertainty	Description	Magnitude
$f_{p1_{cal}}$	Systematic error in calibration of inlet transducer	$\pm 0.0142\%$
$f_{p2_{cal}}$	Systematic error in calibration of outlet transducer	$\pm 0.0634\%$
f_{p1_l}	Random error in the measurements	$\pm 1.71013 \cdot 10^{-5}\%$
f_{p2_l}	Random error in the measurements	$\pm 7.238 \cdot 10^{-5}\%$

Table 5.6: Uncertainty in the pressure measurements.

5.2.2 Uncertainty in the flow rate measurements

The significant uncertainties present in the flow rate measurements were the uncertainty from the calibration, $f_{Q_{cal}}$, and the random error in the measurement, f_{Q_l} , and their values are listed in Table 5.7.

Uncertainty	Description	Magnitude
$f_{Q_{cal}}$	Systematic error in calibration	$\pm 0.5915\%$
f_{Q_l}	Random error in the measurements	$\pm 2.9599 \cdot 10^{-5}\%$

Table 5.7: Uncertainty in the volume flow rate measurements.

The total uncertainty of the flow rate measurements was found by inserting the listed uncertainties into Equation 5.11.

$$f_Q = \pm \sqrt{(f_{Q_{cal}})^2 + (f_{Q_l})^2} = \pm 0.5915\% \quad (5.11)$$

5.2.3 Uncertainty in the torque measurements

The uncertainties significant in the torque measurements was the same as for the flow rate and pressure measurements, listed in Table 5.8.

The total uncertainty for the torque measurements was found with the following equation:

$$f_T = \pm \sqrt{(f_{T_{cal}})^2 + (f_{T_l})^2} = \pm 0.1574\% \quad (5.12)$$

Uncertainty	Description	Magnitude
$f_{T_{cal}}$	Systematic error in calibration	$\pm 0.1574\%$
f_{T_i}	Random error in the measurements	$\pm 1.0809 \cdot 10^{-5}\%$

Table 5.8: Uncertainty in the torque measurements.

5.2.4 Uncertainty in the rotational speed measurements

The systematic uncertainty in the measurements of the rotational speed is stated by the IEC 60193 standard [12] and has the quantity $f_n = f_{n_s} = \pm 0.025\%$. During the testing, the random uncertainty for the rotational speed measurements was found to be $f_{n_i} = 4.1626 \cdot 10^{-5}\%$. The total uncertainty for the rotational speed, measured at 2928 *rpm*, was then calculated as in Equation 5.13.

$$f_n = \pm \sqrt{(f_{n_s})^2 + (f_{n_i})^2} = \pm 0.025\% \quad (5.13)$$

5.3 Uncertainty of the hydraulic efficiency

The uncertainty of the highest measured hydraulic efficiency was found with the SSE-method, combining the uncertainties from the mechanical power, f_P , the flow rate, f_Q , and the hydraulic energy, f_E [16]. A more detailed description and calculation of the uncertainty for the hydraulic efficiency measurement can be found in Appendix C.

$$f_P = \pm \sqrt{(f_T)^2 + (f_n)^2} = \pm 0.1594\% \quad (5.14)$$

$$f_E = \pm \frac{e_E}{E} = \left(\frac{\sqrt{\left(\frac{e_{p1}}{\bar{p}}\right)^2 + \left(\frac{e_{p2}}{\bar{p}}\right)^2 + \left(\frac{e_{v1}^2}{2}\right)^2 + \left(\frac{e_{v1}^2}{2}\right)^2}}{\frac{p_2 - p_1}{\bar{p}} + \frac{v_2^2 - v_1^2}{2}} \right) = \pm 0.3993\% \quad (5.15)$$

$$f_{\eta_h} = \pm \frac{e_{\eta_h}}{\eta_h} = \pm \sqrt{(f_Q)^2 + (f_E)^2 + (f_P)^2} = \pm 0.7308\% \quad (5.16)$$

Chapter VI

Results

The main objective of this thesis was to find the hydraulic efficiency for the centrifugal pump and its pump characteristic presented as an HQ-curve. This chapter presents the results obtained from testing, along with other relevant observations and results. Due to the failure of the pump casing during the tests and a limited amount of time, only a few measurements were conducted for operational points far away from designed conditions.

6.1 Results from the measurements

In this section, the resulting pump characteristics are presented. The pump characteristics are presented as HQ-curves and a comparison between the measured data and the affinity laws have been conducted. Also included in this section are the efficiency curves for each rotational speed, the corrected HQ-curves with the estimated pressure drop in the pipe bend, and other observations during testing.

6.1.1 HQ-curves

The pump characteristics were found by performing five measurement procedures according to the rotational speeds and flow range tabulated in Table 6.1. The testing was conducted according to the procedure found in Appendix D, and the flow rate, torque, rotational speed, and pressure were measured.

Figure 6.1 shows the resulting HQ-curves. Each curve contains five data points except the last curve for 2928 *rpm*, where the experiment had to be stopped as leakage occurred through the weld of the pump casing. Due to this incidence, it was not possible to test for higher rotational speeds and closer to designed conditions. Reading the curve for 2540 *rpm* in Figure 6.1, the maximum head reached during the testing was approximately 19 *m*, with an inlet and outlet pressure of 3.5 *bar* and 5.3 *bar*, respectively.

Measurement	n [rpm]	Range of Q [l/s]	Range of H [m]
1	1206	2.3 – 8.4	-9.13 – 3.63
2	1896	4.3 – 12.2	-15.47 – 8.69
3	2176	5.8 – 13.9	-19.07 – 10.2
4	2540	3.9 – 15.3	-19.50 – 18.68
5	2982	3.9 – 16.9	-19.95 – 11.69

Table 6.1: Test matrix for the measurements.

The affinity laws were calculated and plotted for each HQ-curve, and the result can be seen in Figure 6.2. The laws were implemented to estimate new points on the measured HQ-curves. By scaling the parameters measured for one rotational speed, H and Q , the predicted head and flow rate was found for the other curves. Figure 6.2 shows how the scaled points align with the curves with varying degrees of deviation. Figure 6.3 shows the comparison of the HQ-curves for all rotational speeds obtained from the measurements and the curves fitted with the affinity points. The fitted curves covers an extended predictive range for the measured HQ-curves.

Table 6.2 describes the values for the head deviation between the measured and approximated HQ-curves. Each measured data point is listed with the associated magnitude for the head deviation, denoted ΔH , according to the measured rotational speed. It was discovered that the most evident error yields for 1206 rpm and 2928 rpm.

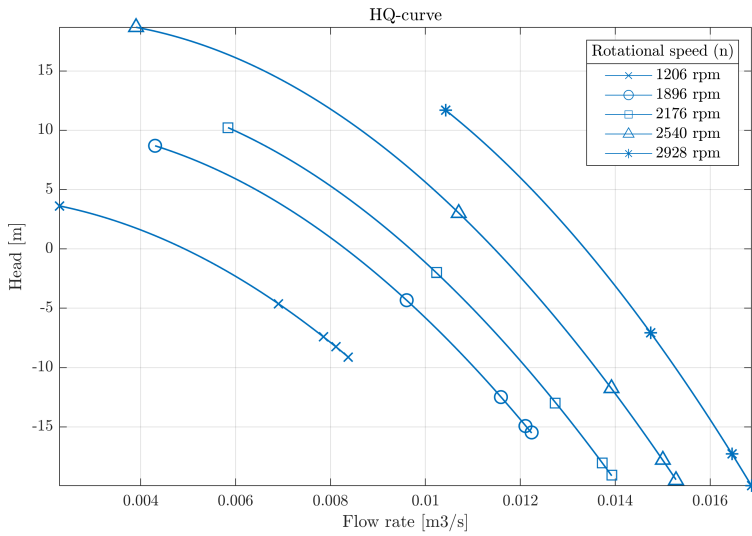


Figure 6.1: HQ-curves obtained from testing.

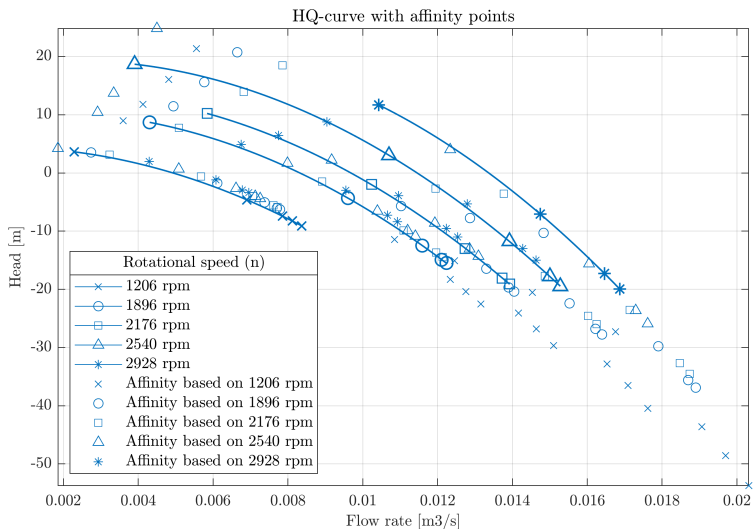


Figure 6.2: Data points scaled using the affinity laws.

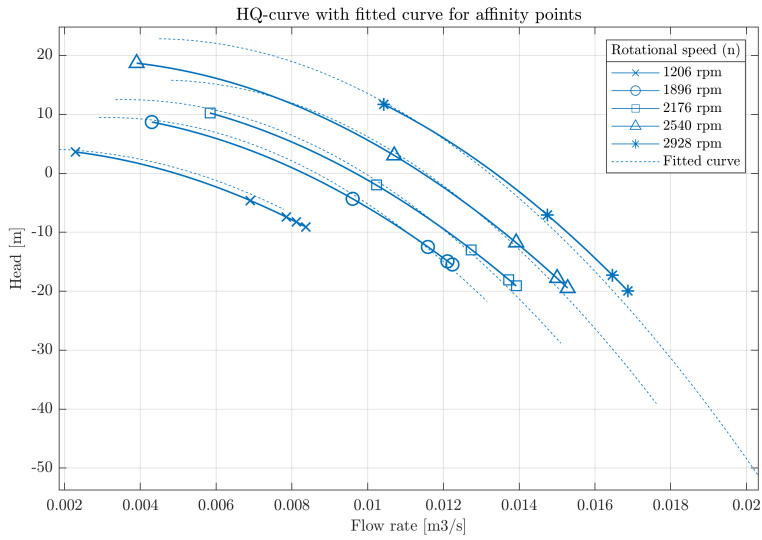


Figure 6.3: The measured HQ-curve compared to the fitted line using the affinity laws.

n [rpm]	Head deviation ΔH [m] in measured point				
	1	2	3	4	5
1206	1.0358	1.0624	1.0848	1.1199	0.2796
1896	0.7887	0.6830	0.2948	0.7746	0.3417
2176	1.7013	1.5098	0.6522	0.7697	0.7086
2540	1.7541	1.5071	0.6743	0.5562	2.9793
2928	2.7986	2.5338	1.5188	0.4065	

Table 6.2: Deviation between measured head and head found with affinity laws.

6.1.2 Hydraulic efficiency

The hydraulic efficiency was computed and plotted as a function of the flow rate, Q , and the result can be seen in Figure 6.4. The efficiency was plotted for each rotational speed with a second-order approximation for the data points. The parameters for the BEP found for each rotational speed are listed in Table 6.3. The maximum hydraulic efficiency found from the testing was 42.29% at a rotational speed of 2928 rpm, which deviates from the maximum efficiency obtained with the approximated curves in Figure 6.4.

n [rpm]	η_{BEP} [%]	Q_{BEP} [l/s]	H_{BEP} [m]
1206	18.42	2.3	3.63
1896	32.53	4.3	8.69
2176	39.60	5.8	10.22
2540	35.75	3.9	18.68
2928	42.29	10.4	11.69

Table 6.3: BEP for each rotational speed obtained from the measurements.

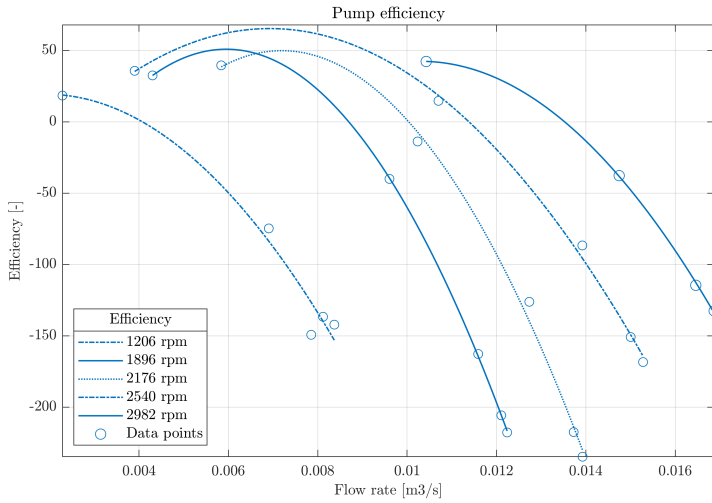


Figure 6.4: Efficiency curves approximated from measured data.

6.1.3 Pressure drop in 90° bend

New values for the pump head was calculated after correcting the outlet pressure, considering the pressure drop through the 90° bend. Figure 6.5 shows the relative head deviation, $\Delta H/H_{measured}$, as a function of the flow rate, after estimating a new outlet pressure. The head showed an increase for all curves. Figure 6.6 illustrate the comparison between the measured and corrected HQ-curve for 2176 rpm, indicating that despite the increase, the head remained negative for higher flow rates. The corrected HQ-curves plotted for the remaining rotational speeds may be seen in section B.1.

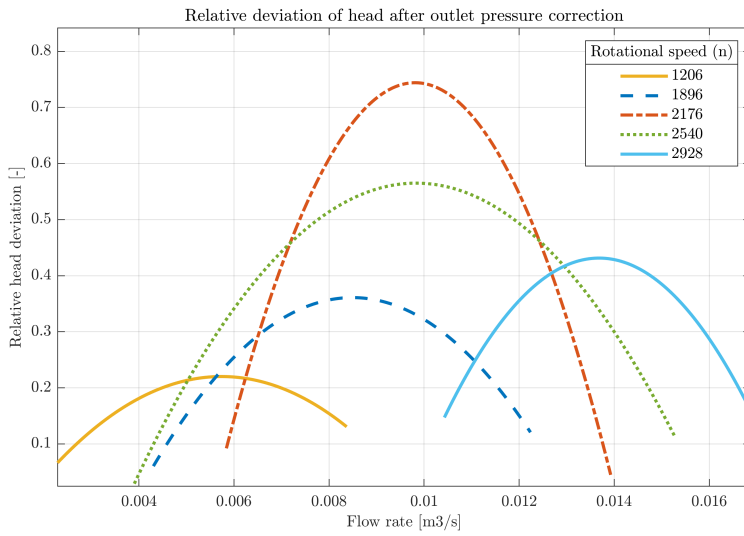


Figure 6.5: Relative deviation for the head.

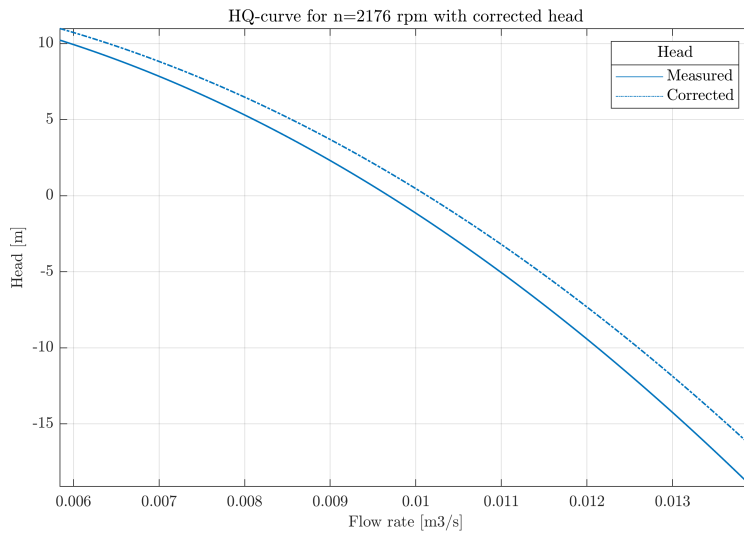


Figure 6.6: Measured and corrected HQ-curves compared for 2176 rpm.

6.1.4 Observations during testing

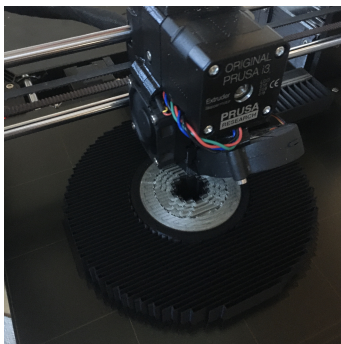
During testing, cavitation noise was detected. The sound of imploding bubbles was clear for the first measurement points at each rotational speed and higher flow rates. An attempt to avoid this noise was carried out by adjusting the inlet pressure with the feed pump in the basement. Despite the adjustment of the inlet pressure, some cavitation noise was still present at the first measurement points for each rotational speed at higher flow rates and lower heads values.

Leakage was detected in the back of the pump, going through the bearing mounted outside the pump casing. The leakage was handled by connecting another drainage tube at one of the flush ports of the pump casing, as no leakage should occur at this part of the pump. After connecting the drainage tube, the water stopped leaking through the outer bearing.

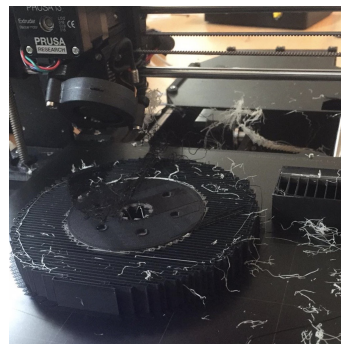
6.2 3D printed impeller

As mentioned in chapter 4, the manufacturing of the impeller was delayed, and additive prototyping was applied to produce a possible model impeller. The attempt to print the impeller using the PLA and the water-soluble filament was challenging as the printer stopped in between switching the filament, or the filament was not attaching properly to the printing surface, as seen in Figure 6.7(b). Since the manufactured impeller came in time for the testing, the procedure for 3D-printing the impeller did not proceed as this was time-consuming and no longer necessary.

A general procedure for 3D-printing was produced and may be found in Appendix E.



(a) 3D print with PLA and water-soluble filament.



(b) Filament fails to attach to the surface.

Figure 6.7: 3D printing of the impeller.

Chapter VII

Discussion

In this chapter, the results presented in chapter 6 will be discussed. Due to several complications during testing regarding the test rig and the centrifugal pump, a discussion for possible improvements is also included.

7.1 Discussion of the measurements

This section discusses the resulting HQ-curves, the affinity laws, and the efficiency curves presented in chapter 6. The estimated pressure drop through the 90° bend is also discussed in this section.

7.1.1 HQ-curves

From the HQ-curves in Figure 6.1, it appears that the head is negative for all curves at the upper range of the measured flow rate, indicating a lower outlet pressure compared to the inlet pressure. As the purpose of the centrifugal pump is to increase the pressure from the suction side to the pump outlet, it is clear that the centrifugal pump did not perform as expected considering the HQ-curves.

One assumption regarding the cause for the low outlet pressure is the installation of the pressure transducer. The pressure transducer was positioned a length 124.5 mm downstream the bend on the outlet pipe, a point where the flow is disrupted and can cause inaccurate pressure measurements. Therefore, it is reasonable to assume that the poorly installed pressure transducer could be a potential contributor to the negative head seen in the pump characteristics.

The measurements were conducted at operational conditions far from design point, which introduce another consideration regarding the negative head. It remains uncertain how the pump performance would be for a designed rotational speed at 10 000 rpm, but it was observed that the head was still negative for higher values

of the rotational speeds and flow rates. It is also assumed that the manual valve on the outlet pipe did not provide sufficient resistance to the flow when operating at high flow rates and contributed to the low outlet pressure.

Although the HQ-curves tend to show similar behavior for various rotational speeds, some areas of the curves are unknown. When restricting the flow by closing the manual valve on the outlet pipe, five equal increments on the valve was utilized. By studying the data points at different flow rates in one of the curves in Figure 6.1, it shows that the valve did not operate linearly. The two last measured data points have a considerably broader difference in flow rate compared to the first measured points. Therefore, the pump characteristics are more uncertain for the lower range of the flow rate.

Before recording the last data point for 2928 *rpm* and presumably a higher head than 19 *m*, the weld on the pump casing failed. This observation indicates that the centrifugal pump only withstands pressures below 5.3 *bar* and is not yet fit for the designed outlet pressure of 20 *bar*.

7.1.2 Affinity laws

Figure 6.2 shows the HQ-curves along with the calculated affinity points. The figure indicates a deviation between the points and the curves with varying degrees. When considering the errors presented in Table 6.2, it can be assumed that the error grows for curves further away from the considered rotational speed. By evaluating the errors with the approximated curves in Figure 6.3, the head deviation in the first measurement point tends to be the most significant. The affinity points scaled from 1206 *rpm* are located far from the measured HQ-curves, and therefore the deviations between the curves are more significant in these areas.

7.1.3 Hydraulic efficiency

The efficiency curves presented in Figure 6.4 follows the same pattern as the HQ-curves, being negative for higher flow rates. The efficiency should certainly not be negative and is a consequence of the negative pressure difference through the centrifugal pump. Again, it is unknown how the efficiency would appear closer to designed conditions, but the curves show a consistent negative behaviour when increasing the rotational speed.

The efficiency curves were plotted with a second-order approximation against the measured data points. The approximated curves for 1896 *rpm*, 2176 *rpm*, and 2540 *rpm* show a considerably higher maximum efficiency compared to the maximum measured efficiency. If the peaks of these curves comply with the real efficiency for these flow rates remains uncertain as the range between the measured

data points is strikingly large. Despite this uncertainty, it is assumed that efficiency for the curve at 2928 *rpm* would reach a higher efficiency if the last data point was recorded.

The maximum efficiency found during the measurements was 42.29% at 2928*rpm*. The efficiency is considered to be low as the centrifugal pump was operating far from its designed conditions. Evaluating the observations during testing, both the cavitation and the leakage could have impaired the efficiency. Without knowing the magnitude of the cavitation, such occurrence could cause flow disruption and increases hydraulic losses at developed cavitation. The leakage detected at the back part of the pump casing could also have affected the efficiency in terms of leakage losses. As the flow was measured before the outtake for the flush port, the flow measurement indicates a higher flow rate than supplied at the inlet.

7.1.4 Pressure drop in 90° bend

When accounting for the pressure drop in the 90° bend, Figure 6.6 indicate a deviation in the pump characteristics for the rotational speed of 2176 *rpm*. The same pattern of deviation was discovered for the other rotational speeds presented in Appendix B.1. Despite the correction of the outlet pressure, the head and efficiency was still negative for the higher flow rates. This observation may indicate that the pressure measurement were affected by the installment of the pressure transducer, but is it not assumed to be the critical factor for the negative pressure difference through the pump.

7.2 Discussion of uncertainty analysis

The uncertainty analysis, introduced in chapter 5, resulted in total relative uncertainty of $\pm 0.6638\%$ for the maximum measured hydraulic efficiency. The absolute uncertainty of the hydraulic efficiency is then $\pm 0.3090\%$.

Considering the relative errors used to calculate the uncertainty with the RSS-method, the most significant contribution originates in the uncertainty in the flow rate measurements. By studying f_Q with the uncertainties from both calibration and measurements, it is evident that the magnitude of the regression error, $f_{Q_{regression}}$, provide the most significant impact on the calibration uncertainty $f_{Q_{cal}}$. Figure 7.1 show the magnitude of the regression error compared to the other errors contributing to the flow meter calibration. The regression error for the measured flow at 10.4 *l/s*, is assumed to be large due to testing in the lower range for the flow meter.

Also, the regression error from the calibration of the torque transducer and the pressure transducers, $f_{T_{regression}}$ and $f_{p_{regression}}$, was the major contributor to the uncertainty in the efficiency, but not with the same magnitude as for $f_{Q_{regression}}$.

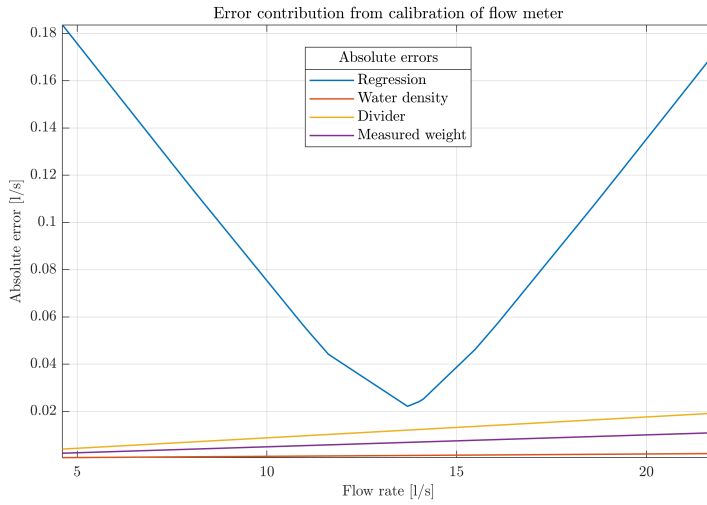


Figure 7.1: Errors present when calibrating the flow meter.

7.3 Discussion of possible improvements

Due to numerous difficulties during the tests, both with the measurements and the pump failure, it is clear that certain improvements must be carried out before the experiment continues. In this section, improvements for both the centrifugal pump and the test rig are suggested.

7.3.1 Centrifugal pump

Impeller

The outer diameters on the impeller were inspected before mounting it inside the pump casing. It was detected an imbalance, as some geometric dimensions were varying with a couple of tenths. An imbalance of the impeller indicates a skewness in the mass distribution, which leads to vibrations during high rotational speeds. Due to a limited amount of time, the testing was conducted with the imbalanced impeller. Therefore, it is recommended that the impeller undergo a balance test, and is adjusted accordingly, before future testing.

The impeller was initially manufactured in two parts and then assembled by soldering. The soldering process caused an increased width. Thus, the clearance between the impeller and the suction eye of the casing was shortened. The reduced clearance generated surface friction at the interference, leading to high resistance when trying to rotate the impeller shaft. A recommended clearance between the impeller and casing should not exceed 0.05 to 0.15 *mm* [1], and this should be assured before further testing.

Casing

The leakage from the pump casing caused by cracks in the weld is a critical issue. The cracks appeared below designed values for the outlet pressure, indicating a non-sufficient weld. As a centrifugal pump may have some leakages through the seals, no leakage should occur through the walls of the casing. It is recommended to carry out a pressure test on the centrifugal pump to check for leakages and material deformation at values above maximum expected pressure.

Leakage

During testing, a leakage was detected on the back part of the pump casing, going through a radial seal on the impeller shaft. Leakage flow, earlier discussed in section 2.3, contributes to higher hydraulic losses and leads to lower efficiencies. Due to time limitations throughout this study, it was not prioritized to find a new seal before executing the experiments. However, no leakage should occur through this part of the pump, and it is recommended to examine the seal further.

7.3.2 Test rig

Torque measurement

The power transmission was achieved through a geared belt drive system, increasing the rotational speed with a ratio of 8 from the engine shaft to the impeller shaft. Such a belt installation comes with mechanical losses that cannot be measured without a second torque transducer at the impeller shaft. A possible improvement would be to measure the torque at the impeller shaft for a more accurate torque measurement and decide the mechanical losses through the belt drive as shown in Equation 7.1.

$$\eta_m = \frac{T_{impeller} \cdot n_{impeller}}{T_{engine} \cdot n_{engine}} \quad (7.1)$$

Installation of outlet pressure transducer

The pressure transducer used to measure the outlet pressure was installed after the bend on the outlet pipe. According to the IEC 60193 standard [12], the installation of the pressure transducer must avoid bends to assure a uniform flow. As this installation is assumed to impact the outlet pressure and the negative head, an improvement should be to install the pressure transducer at the horizontal part of the outlet pipe before the bend.

Manual valve

It is assumed that the manual valve on the outlet pipe was not sufficient to achieve the desired outlet pressure when restricting the flow. An additional detection was the non-linear behavior of the valve when adjusting the flow rate with equal increments. The non-linearity caused a large spacing between the last data points at low ranges of the flow rate, and the pump characteristics and efficiency became more uncertain in this range. Therefore, an improvement of the test rig would be to install a new valve for regulating the flow rate, which operates linearly and assures adequate resistance.

Detection of cavitation

As mentioned, cavitation noise was detected during the testing. For further investigation of cavitation a possible improvement for the rig is to install a transparent cone at the low pressure side where cavitation normally occurs, i.e., the pump inlet section. A transparent cone gives the opportunity to observe the cavitation pattern combined with stroboscopic light [12]. One must assure that the possible installed transparent cone can withstand the designed inlet pressure of 5 bar.

Chapter VIII

Conclusion

In this thesis, hydraulic efficiency measurements on a centrifugal pump have been conducted and presented in an HQ-diagram. The centrifugal pump was the first prototype of its kind to be tested in the laboratory. Therefore, it was also essential to perform the tests to assure that the pump design was verified for its designed parameters.

The centrifugal pump was tested in the Waterpower Laboratory using a test rig designed for this study, with instrumentation for measuring the pressure, torque, volume flow rate, and rotational speed. All the instrumentation was calibrated in advance to reduce the uncertainty in the measurements. After the testing, a procedure for operating the centrifugal pump test rig was produced, as the rig was a new installation at the Waterpower Laboratory. Due to a significant delay in the manufacturing process of the impeller, it was attempted to 3D-print a possible model impeller. The process did not continue since the original impeller finished in time. A procedure for 3D-printing was also produced.

The presented study revealed that the centrifugal pump was not able to withstand its designed pressure. The pump casing cracked, and leaks occurred near the outlet, operating at an outlet pressure slightly above 5.3 *bar*. Due to this failure, the tests were stopped, and the pump was only tested for rotational speeds up to 2928 *rpm*. The maximum hydraulic efficiency found was 42.29 %, and is assumed to be reasonably low since the pump was operating far from its best operational point.

An additional issue during testing was the negative pressure difference from inlet to outlet, occurring for higher flow rates at all rotational speeds. This caused a negative head and efficiency for several recorded data points. As the outlet pressure transducer was inadequately installed, the pressure loss through the bend was estimated. The corrected head and efficiency was slightly higher but still negative for multiple points. The cause of the negative pressure difference remains

uncertain. However, the valve to regulate the flow rate at the outlet pipe should be considered replaced to assure a sufficient resistance for the outlet pressure.

Based on the results from this experiment, it can be concluded that the centrifugal pump design is not verified. As the pump is designed for an outlet pressure of 20 bar , a pressure test should be performed on the pump before continuing the testing. The pressure transducer must be correctly installed, and the manual valve should be investigated. After carrying out the suggested improvements, it is possible to decide if the pump can deliver the correct outlet pressure and to determine the hydraulic efficiency at designed operational conditions.

Chapter IX

Further work

This chapter will introduce the further work suggested based on the conclusion of this study, the recommended improvements in chapter 7, and the work that was left out from the experiment due to a limited amount of time.

9.1 Future testing

After the improvements of the centrifugal pump and the test rig have been carried out, further testing should be conducted in order to obtain a more reliable pump characteristic and efficiency. Listed below are the highlighted improvements to be implemented before continuing the testing of the centrifugal pump.

- The pressure transducer should be relocated to the horizontal part of the outlet pipe before the bend to assure more accurate measurement of the outlet pressure.
- The manual valve used to regulate the flow rate, mounted on the outlet pipe, should be replaced. To use a valve with a more linear behavior would give a more precise result of the pump characteristic and efficiency. After relocating the pressure transducer and replacing the manual valve, it can be evaluated if this was the cause for the low outlet pressure.
- The impeller imbalance should be corrected, as an imbalance can cause vibrations during high rotational speed.
- The pump must undergo a pressure test before any further testing. This is highly recommended as several leakages and cracks appeared during the testing, and it must be assured that the material and the selected seals can withstand the required pressure while running.

9.2 Evaluation of flow phenomena

Due to a limited amount of time caused by production failure and postponement of laboratory work, the study of flow phenomena regarding hydraulic turbomachinery was left out. This section suggests some phenomena that should be examined during future testing.

- Cavitation noise was detected during this experiment, for high flow rates and low heads. Further investigation of cavitation in the centrifugal pump is necessary, as the presence of imploding bubbles cause material fatigue and can damage to the impeller blades.
- Pressure pulsations were not examined during this study. For future testing, it is recommended to determine the magnitude of the pulsations, as this phenomena cause damage to the hydraulic system and the pipes.

References

- [1] Gülich, J. F., 2014, *Centrifugal Pumps*, Springer.
- [2] Kjølle, A., 2003, *Hydraulisk Måleteknikk*, NTNU.
- [3] Brekke, H., 2000, *Grunnkurs i hydrauliske Strømningsmaskiner*, Waterpower Laboratory NTNU.
- [4] Dahlhaug, O. G., 2006, *Francis99*, NTNU internal.
- [5] Anderson, H. H., 1994, *Centrifugal pumps and allied machinery*, Elsevier.
- [6] Sakserud, N. M. K., 2019, “Centrifugal Pump For a Rocket Engine,” Master’s thesis, NTNU.
- [7] Dick, E., 2015, *Fundamentals of Turbomachines*, Springer.
- [8] Veie, C. A., 2018, “Dynamics analysis of a system with RPT,” Master’s thesis, NTNU.
- [9] Wnek, T. F., 1987, “Pressure pulsations generated by centrifugal pumps,” Tech. rep., Warren Pumps Inc.
- [10] Øyvind Antonsen, 2007, “Unsteady flow in wicket gate and runner with focus on static and dynamic load on runner,” Ph.D. thesis, NTNU.
- [11] Solemslie, B. W., 2010, “Optimalisering av ringledning for Pelton turbin,” Master’s thesis, NTNU.
- [12] International Electrotechnical Commission, 2019, “IEC 60193: Hydraulic turbines, storage pumps and pump-turbines – Model acceptance test,” Standard, IEC, Geneva, Switzerland.

- [13] Walpole, R. E., 2012, *Probability Statistics For Engineers and Scientists*, Pearson.
- [14] Stene, I. B., 2014, "Design of a Pelton Model Test Rig at Kathmandu University," Master's thesis, NTNU.
- [15] Company, B. . W., 2005, *Steam: its generation and use*, Babcock & Wilcox Company.
- [16] Storli, P. T. S., 2006, "Modelltest av Francis turbin i Vannkraftlaboratoriet ved NTNU," Master's thesis, NTNU.

Appendix - A

Calibration procedures

This appendix will present a more detailed description of the calibration procedures used for the instrumentation installed in the centrifugal pump test rig. A calibration report from each procedure completed is also included. The laboratory has established procedures for calibration according to the IEC 60193 standard [12].

The following calibration procedures can be found in this appendix:

- A.1 Weighing tank
- A.2 Flow meter
- A.3 Torque transducer
- A.4 Pressure transducers

A.1 Calibration procedure for weighing tank

Wait until the recording is stable for each measurement point, approximately 200s and a low standard deviation.

Procedure

1. Remove the weights, record the weight of the tank. The logging program will let you know if the weight should be put on or off.
2. Add the weights, unhook the crane and lift it above the weight so it does not interfere with the weight measurement. Wait for the system to stabilize and record.
3. Repeat step 1 and 2 once, then go to step 4.
4. Activate the tilt screen to fill the tank.
5. Go back to step 1 and do a new set of measurements with the new base load.


It is desired to measure the delta m (weight on - weight off) twice per base load.

Calculation

The calibration function for the weighing tank results in a fifth order polynomial. The function W represents the relationship between the amplifier reading c and the applied weight in the force transducers.

$$W = a_0 \cdot \frac{c^5}{5} + a_1 \cdot \frac{c^4}{4} + a_2 \cdot \frac{c^3}{3} + a_3 \cdot \frac{c^2}{2} + a_4 \cdot c \quad (\text{A.1})$$

The coefficients is found by using an Excel template made at the Waterpower Laboratory and the calibration report can be found on the next page.

	WATERPOWER LABORATORY NTNU	Date: 14.01.2020
	Calibration Sheet	Sign operator: Rakel Heggset Gro Mari K. Langlete
	Calibration of weighing tank load cells	Approved:

Unit: Weighing tank load cells, reg. nr. 4331-5/6/7

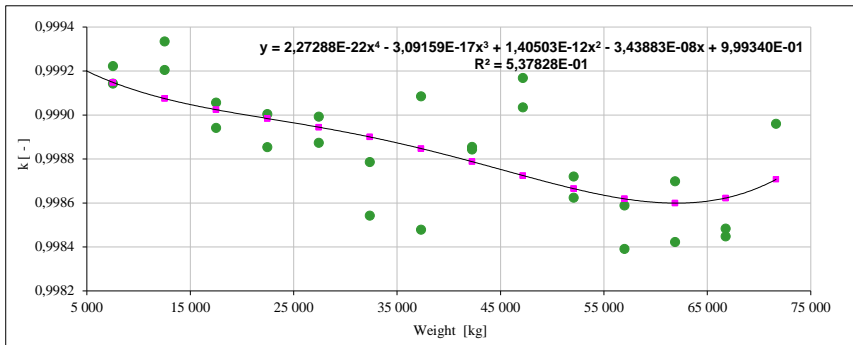
Weight W_L 5126,075 [kg]

Comments:

Manual Observation	Manual Observation	Displayed load increase	$k = \frac{W_L}{\Delta W}$	Weight midpoint	Estimated correction factor	Difference in real k and estimated k	
						Dk	Dk
Weights off	Weights on	DW	k	Weight	k	[-]	[%]
[kg]	[kg]	[kg]	[-]	[kg]	[-]	[-]	[%]
-20,9	5110,2	5131,05071	0,9990	2544,6	0,99926	0,00023	0,023
-19,5	5110,1	5129,542614	0,9993	2545,3	0,99926	-0,00006	0,006
4967,1	10097,1	5130,060743	0,9992	7532,1	0,99915	-0,00007	0,007
4966,6	10097,1	5130,470193	0,9991	7531,9	0,99915	0,00000	0,000
9949,9	15080,0	5130,151303	0,9992	12514,9	0,99907	-0,00013	0,013
9950,0	15079,5	5129,487267	0,9993	12514,7	0,99907	-0,00026	0,026
14919,9	20051,4	5131,508005	0,9989	17485,7	0,99902	0,00008	0,008
14921,6	20052,5	5130,916153	0,9991	17487,1	0,99902	-0,00003	0,003
19887,9	25019,1	5131,184711	0,9990	22453,5	0,99898	-0,00002	0,002
19887,1	25019,0	5131,956242	0,9989	22453,1	0,99898	0,00013	0,013
24854,0	29985,2	5131,24601	0,9990	27419,6	0,99894	-0,00005	0,005
24853,0	29984,9	5131,853622	0,9989	27418,9	0,99894	0,00007	0,007
29798,7	34931,0	5132,304835	0,9988	32364,9	0,99890	0,00011	0,011
29797,7	34931,3	5133,555252	0,9985	32364,5	0,99890	0,00036	0,036
34744,3	39875,1	5130,769687	0,9991	37309,7	0,99885	-0,00024	0,024
34741,8	39875,7	5133,885115	0,9985	37308,8	0,99885	0,00037	0,037
39675,3	44807,2	5131,95191	0,9989	42241,2	0,99879	-0,00007	0,007
39674,5	44806,5	5132,010664	0,9988	42240,5	0,99879	-0,00006	0,006
44596,2	49726,5	5130,34298	0,9992	47161,4	0,99872	-0,00044	0,044
44595,6	49726,6	5131,028497	0,9990	47161,1	0,99872	-0,00031	0,031
49513,4	54646,5	5133,138535	0,9986	52079,9	0,99867	0,00004	0,004
49513,6	54646,2	5132,643261	0,9987	52079,9	0,99867	-0,00006	0,006
54418,3	59551,7	5133,317331	0,9986	56985,0	0,99862	0,00003	0,003
54417,4	59551,7	5134,334417	0,9984	56984,5	0,99862	0,00023	0,023
59313,5	64446,3	5132,755867	0,9987	61879,9	0,99860	-0,00010	0,010
59312,1	64446,3	5134,17318	0,9984	61879,2	0,99860	0,00018	0,018
64196,5	69330,5	5134,044354	0,9984	66763,5	0,99862	0,00017	0,017
64196,3	69330,2	5133,858643	0,9985	66763,3	0,99862	0,00014	0,014
69076,6	74208,0	5131,410017	0,9990	71642,3	0,99871	-0,00025	0,025

Calibration constants	a ₁	2,27288E-22		
	a ₂	-3,09159E-17		
	a ₃	1,40503E-12		
	a ₄	-3,43883E-08		
	a ₅	9,99340E-01		
a1	a2	a3	a4	a5

2,27288E-22 -3,09159E-17 1,40503E-12 -3,4388E-08 0,999340073



A.2 Calibration procedure for flow meter

The flow meter was calibrated using the weighing tank system in the Waterpower Laboratory. The weighing tank consist of several load cells manufactured by Hottinger and the flow meter is of the type Krohne Optiflux 2300C with a signal converter giving an output signal in V . A manual valve right before the weighing tank was used to regulate the flow rate.

By recording the weight of the tank before and after, and the time of filling, the flow rate through the flow meter is found. These three recordings represent one measurement point.

Procedure

1. Adjust the manual valve to obtain the flow rate for the measurement point.
2. Record the weight of the water in the tank before activating the tilting screen.
3. Set a desired filling time before activating the tilting screen. It should be estimated so that the tank is filled with 5 tons of water during each filling. The filling time will change for different flow rates.
4. Activate the tilting screen and wait for the tank to be filled with water. After the tilting screen deactivates, record the measured data for the flow rate. One must also register the *actual* filling time due to a time lag in the tilting screen. Air and water temperatures and the atmospheric pressure are also registered. This is done for each measuring point of the flow rate.
5. Record the weight of the water in the tank after filling.
6. Repeat the process until enough measurement points are obtained for a sufficient calibration curve. 7 points within the range of the expected flow rate is recommended and should be repeated up and down two times.

Calculation

Before calculating the volume flow rate, Q , one must use the calibration constant obtained from the weighing tank calibration to find the corrected mass before and after filling. The correction equation is Equation A.1 in section A.1. The air and water density is corrected with Equation A.3 and Equation A.2, respectively.

$$\rho_w = \frac{10^3}{(1 - 4.6699 \cdot 10^{-10} \cdot p) + 8 \cdot 10^{-6} \cdot (\theta_w - 4 + 2.1318913 \cdot 10^{-7} \cdot p)^2 - 6 \cdot 10^{-8} \cdot (\theta_w - 4 + 2.13118913 \cdot 10^{-7} \cdot p)^3} \quad [kg/m^3] \quad (A.2)$$

$$\rho_{amb} = \frac{p_{atm} \cdot 3.4837 \cdot 10^{-3}}{273.15 + \theta_{amb}} \quad [kg/m^3] \quad (A.3)$$

Here, p is the absolute pressure in Pascal, θ_w is the water temperature, p_{atm} is the atmospheric pressure and θ_{amb} is the ambient air temperature. The mean volume flow rate, Q , is then calculated with Equation A.4

$$Q = \frac{W_2 - W_1}{\rho_w \cdot t \cdot \left(1 - \frac{\rho_{amb}}{\rho_w}\right)} \quad [m^3/s] \quad (A.4)$$

where t is the measured time for filling the weighing tank. The calibration report of the flow meter may be found on the following page.

Calibration of flow meter

Operator: Rakel Heggset

Flow meter: Krohne Optiflux 2300C

Poly fit equation: $Y = 0.002834 * x - 0.006306$

WeightBefore	WeightAfter	FlowVoltage	Time	Pair	Twater	Tair	SDbefore	SDafter
3975.360916	8886.437984	3.986751859	995.101	98.966	15.38	19.42	0.058374041	0.043904945
8886.464023	13581.00294	5.101349735	577.108	99.007	14.92	19.52	0.049591019	0.048841655
13580.91336	18311.83997	6.171702863	432.105	99.007	14.77	19.41	0.048490543	0.047465216
18311.73059	23139.77755	7.165458434	348.103	99.03	14.7	19.38	0.040538999	0.057901409
27964.18084	32971.6249	7.899743453	308.105	99.07	14.76	19.41	0.03412978	0.074724315
32971.46139	37958.38352	9.076077051	261.106	99.079	14.72	19.3	0.057193702	0.080056903
37958.04866	42886.87383	9.770883794	230.107	99.086	14.78	19.37	0.044742919	0.130143057
42886.47718	47898.41994	9.911744561	230.107	99.102	14.77	19.37	0.04084717	0.096595875
47898.09029	52815.98941	8.90719584	261.107	99.112	14.84	19.35	0.051215743	0.050063989
52815.83752	57764.45789	7.904078117	308.107	99.126	14.85	19.41	0.035128312	0.098202988
57764.12676	62748.75715	7.208941712	348.106	99.13	14.86	19.46	0.049282185	0.083434463
62748.32887	67695.37322	6.159644066	434.106	99.141	14.91	19.51	0.044287533	0.076644856
5977.957374	10881.88884	4.996586413	597.105	99.184	14.98	19.4	0.058100083	0.056018558
10881.7459	15510.8277	4.117035429	929.102	99.184	15.24	19.33	0.078927367	0.095779521
15510.84635	20204.8462	3.852225258	951.106	99.205	15.31	19.32	0.090480895	0.068783742
20204.68186	25103.44758	4.945925686	610.108	99.218	15.01	19.36	0.077858951	0.064089492
25103.22303	30019.80703	6.087416491	443.108	99.239	14.91	19.38	0.056974984	0.057384389
30019.701	35021.58109	7.190584761	348.106	99.238	14.88	19.33	0.047527167	0.08236086
35021.41041	40076.36497	7.8846184	308.107	99.24	14.9	19.37	0.047373172	0.068693885
40076.08397	45132.54265	8.874205256	264.112	99.251	14.92	19.38	0.066747269	0.060076783
45132.33037	50079.1813	9.852373501	228.11	99.238	14.89	19.32	0.046677078	0.09771435
50078.88881	55075.8028	9.873879809	230.107	99.244	14.91	19.41	0.060570713	0.077526842
55075.36255	59816.64121	8.779851551	264.107	99.243	14.95	19.46	0.055879991	0.096895016
59816.03896	64481.34241	7.68737875	303.109	99.249	14.96	19.34	0.080097499	0.167416023
41064.17993	45990.84667	7.060691298	358.107	99.277	14.99	19.33	0.15436895	0.075320761
45990.56433	50808.70147	6.326252279	440.105	99.269	15.03	19.3	0.063949049	0.22991077
50809.00402	55216.82438	4.968049311	602.105	99.274	15.08	19.32	0.25539664	0.172299869
55216.98237	59586.65022	3.877778216	948.106	99.278	15.35	19.34	0.092915809	0.183504456

SDflow	Nbefore	Nafter	Nflow
0.109233498	8600	5440	1979346
0.052478199	5040	5000	1157027
0.065571949	4000	6680	867765
0.015678642	4640	5760	700416
0.017895139	2840	5800	622933
0.073922486	4040	6440	528927
0.041839647	4000	12160	459710
0.036449988	6400	6080	463841
0.026338158	2880	6400	527891
0.030653696	4520	6200	617770
0.014112443	4440	6600	702478
0.01946545	2440	6960	869837
0.024955611	5280	2320	1195251
0.133228113	4280	8160	1871906
0.005762382	6640	4920	1912193
0.013976076	6200	3720	1217979
0.015795213	2360	6040	888434
0.020750371	2720	5160	710748
0.015173416	2960	4600	617771
0.014626092	4560	1960	527891
0.020342252	4000	5160	456613
0.022842341	3120	3000	460742
0.147597698	1960	2680	526861
0.113487106	13080	9480	607436
0.014280702	4800	4680	729339
0.354608139	3280	8120	883266
0.041118528	7200	9360	1210745
0.009682574	5920	6400	1901867

A.3 Calibration procedure for torque transducer

The torque transducer is calibrated using a lever mounted onto the shaft that is kept from rotating. A fixture is attached at the end of the arm and numerous calibrated weights are loaded onto the fixture to create a force F . The lever arm is mounted onto the shaft with a centered position so that the force from the arm it self is counter-balanced.

The torque transducer gives an output value in Volts and must be calibrated against a primary method. The torque was calibrated by applying a force $F = m \cdot g$ to a lever arm mounted to the engine shaft that was kept from rotating. The force applied to the arm was measured by loading weights on a fixture attached to the lever arm with a length $L = 0.5$ from the center. The lever arm was mounted onto the shaft with a centered position so that the force from arm it self was counter-balance. The torque applied on the shaft is measured by Equation A.5.

$$T = F \cdot L = m \cdot g \cdot L \quad [Nm] \quad (A.5)$$

Procedure

1. Connect the torque transducer to the signal converter which must be connected to a logging computer. Fix the engine shaft so that it is kept from rotating and mount the lever arm on the shaft in a centered position.
2. Prepare the fixture and the calibrated weights to be loaded. The weight of the fixture must also be measured as it gives an contribution to the torque. Make sure to have enough weights to exceed the maximum expected torque in the measurements.
3. Do the first recording of the torque with no weights or fixture attached to the lever arm.
4. Do the second recording after attaching the fixture. Make sure there is no pendulum or rotating motion of the fixture when doing the recording.
5. Continue the calibration by loading weights on the fixture and record the voltage signal for each loading. Remember to obtain small increments of the weight in the beginning and end of the calibration curve because of a higher uncertainty in these areas.
6. When reaching maximum weight on the fixture, repeat the procedure by unloading weights. This will produce two recorded points for each weight applied.

7. Continue until all weights are unloaded. Record the volt signal with only the fixture.
8. Remove the fixture and do the last recording with only the lever arm mounted to the shaft.

Calculations

The fixture is attached on the arm a known length L from the torque transducer. The mass of the fixture itself and the mass of the weights creates a force $F = m \cdot g$. The fixture must be weighted and the weights to be loaded have a known weight of 5 kg . The torque is calculated with

$$T = F \cdot L = m \cdot g \cdot L \tag{A.6}$$

The calibration report for the torque transducer can be found on the following page.

CALIBRATION REPORT

CALIBRATION PROPERTIES

Calibrated by: Rakel Heggset

Type/Producer: HBM

SN: 0

Range: 0-660 Nm

Unit: Nm

CALIBRATION SOURCE PROPERTIES

Type/Producer: Calibrated Weights

SN: -

Uncertainty [%]: -

POLY FIT EQUATION:

$Y = +975,79556026E-3X^0 + 101,15407163E+0X^1$

CALIBRATION SUMMARY:

Max Uncertainty : Inf [%]

Max Uncertainty : 0,152592 [Nm]

RSQ : 0,999999

Calibration points : 22

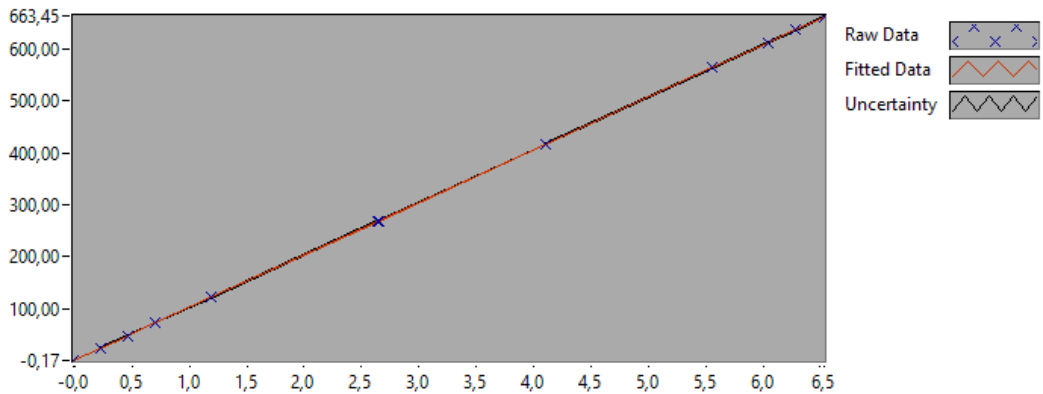


Figure 1 : Calibration chart (The uncertainty band is multiplied by 10)

Rakel Heggset

CALIBRATION VALUES

<u>Value [Nm]</u>	<u>Voltage [V]</u>	<u>Best Poly Fit [Nm]</u>	<u>Deviation [Nm]</u>	<u>Uncertainty [%]</u>	<u>Uncertainty [Nm]</u>
<u>0,000000</u>	<u>-0,008343</u>	<u>0,131858</u>	<u>-0,131858</u>	<u>Inf</u>	<u>NaN</u>
<u>23,225309</u>	<u>0,224274</u>	<u>23,661986</u>	<u>-0,436676</u>	<u>0,583104</u>	<u>0,135428</u>
<u>47,778972</u>	<u>0,461340</u>	<u>47,642178</u>	<u>0,136794</u>	<u>0,270647</u>	<u>0,129313</u>
<u>72,332634</u>	<u>0,706107</u>	<u>72,401393</u>	<u>-0,068758</u>	<u>0,170499</u>	<u>0,123327</u>
<u>121,439959</u>	<u>1,187933</u>	<u>121,140033</u>	<u>0,299927</u>	<u>0,092648</u>	<u>0,112512</u>
<u>268,761934</u>	<u>2,645637</u>	<u>268,592791</u>	<u>0,169143</u>	<u>0,034198</u>	<u>0,091912</u>
<u>416,083909</u>	<u>4,101925</u>	<u>415,902245</u>	<u>0,181664</u>	<u>0,023519</u>	<u>0,097859</u>
<u>563,405884</u>	<u>5,560792</u>	<u>563,472539</u>	<u>-0,066655</u>	<u>0,022453</u>	<u>0,126499</u>
<u>612,513209</u>	<u>6,043756</u>	<u>612,326294</u>	<u>0,186916</u>	<u>0,022689</u>	<u>0,138973</u>
<u>637,066872</u>	<u>6,286286</u>	<u>636,859213</u>	<u>0,207659</u>	<u>0,022844</u>	<u>0,145531</u>
<u>661,620534</u>	<u>6,531497</u>	<u>661,663351</u>	<u>-0,042817</u>	<u>0,023045</u>	<u>0,152467</u>
<u>661,620534</u>	<u>6,534085</u>	<u>661,925109</u>	<u>-0,304575</u>	<u>0,023063</u>	<u>0,152592</u>
<u>637,066872</u>	<u>6,286460</u>	<u>636,876836</u>	<u>0,190036</u>	<u>0,022844</u>	<u>0,145533</u>
<u>612,513209</u>	<u>6,044931</u>	<u>612,445194</u>	<u>0,068015</u>	<u>0,022704</u>	<u>0,139067</u>
<u>563,405884</u>	<u>5,561525</u>	<u>563,546659</u>	<u>-0,140775</u>	<u>0,022451</u>	<u>0,126490</u>
<u>416,083909</u>	<u>4,108319</u>	<u>416,549000</u>	<u>-0,465090</u>	<u>0,023531</u>	<u>0,097908</u>
<u>268,761934</u>	<u>2,648367</u>	<u>268,868931</u>	<u>-0,106997</u>	<u>0,034212</u>	<u>0,091949</u>
<u>121,439959</u>	<u>1,190276</u>	<u>121,377037</u>	<u>0,062922</u>	<u>0,092563</u>	<u>0,112408</u>
<u>72,332634</u>	<u>0,706182</u>	<u>72,409010</u>	<u>-0,076376</u>	<u>0,170417</u>	<u>0,123267</u>
<u>47,778972</u>	<u>0,460476</u>	<u>47,554778</u>	<u>0,224193</u>	<u>0,270725</u>	<u>0,129350</u>
<u>23,225309</u>	<u>0,220512</u>	<u>23,281436</u>	<u>-0,056127</u>	<u>0,583482</u>	<u>0,135515</u>
<u>0,000000</u>	<u>-0,011322</u>	<u>-0,169434</u>	<u>0,169434</u>	<u>Inf</u>	<u>NaN</u>

COMMENTS:

The uncertainty is calculated with 95% confidence. The uncertainty includes the randomness in the calibrated instrument during the calibration, systematic uncertainty in the instrument or property which the instrument under calibration is compared with (dead weight manometer, calibrated weights etc.), and due to regression analysis to fit the calibration points to a linear calibration equation. The calculated uncertainty can be used as the total systematic uncertainty of the calibrated instrument with the given calibration equation.

A.4 Calibration of pressure transducers

To calibrate the pressure transducer a dead weight manometer was used. The manometer was a P3223-1 manometer from GE Sensing. The pressure transducer is connected to the manometer through a tap and calibrated weights are loaded onto a piston with known area. The piston pressurizes a liquid located in the manometer reservoir and the pressure is measured for each new loading of weights.

Procedure

1. Prepare the dead weight manometer and the weights to be loaded onto the cylinder. Mount the pressure transducer to the tap and connect it to the logging device. Make sure to tighten the transducer properly so no leakage occurs. Adjust the leveling feet under the manometer so that it is leveled.
2. Priming
 - (a) Open the valve of the reservoir and turn the screw press fully in.
 - (b) Pump the priming pump two times.
 - (c) Close the valve and turn the screw press all the way out. Bubbles may appear during this operation. Step a and b must therefore be repeated until no bubbles appear.
 - (d) With valve still open, turn the screw press fully out and close the valve.
3. Measure the height difference Z between the pressure transducer and the inlet.
4. The first point is recorded by opening the reservoir valve to depressurize the system. This will be the zero load point. After the recording is done, close the valve.
5. Second point is recorded by raising the circular disc, still with no weights. The manometer is equipped with an indicator showing the reference point of the disc. The liquid is now pressurized with 1 bar. Spin the circular disc to remove frictional effects and record the point when the disk is spinning freely in the horizontal plane. This must be done for every recording point.
6. The next recordings are done by loading weights onto the cylindrical disk until the desired pressure range is reached. Each pressure transducer indicates its range. Always check that the height of the piston stays at the correct point on the indicator.

Calculations

The pressure is calculated with the known area of the piston, A , and the known mass of the loaded weights. The weights indicate a certain pressure

$$p = \frac{F}{A} \quad (\text{A.7})$$

$$F = m \cdot g \quad (\text{A.8})$$

The calibration report for both pressure transducers can be found on the next page.

CALIBRATION REPORT

CALIBRATION PROPERTIES

Calibrated by: Rakel Heggset
Type/Producer: GE Druck
SN: 0
Range: 0-6 bar
Unit: kPa

CALIBRATION SOURCE PROPERTIES

Type/Producer: Pressurements deadweight tester P3223-1
SN: 66256
Uncertainty [%]: 0,01

POLY FIT EQUATION:

$Y = -149,95763094E+0X^0 + 75,01014586E+0X^1$

CALIBRATION SUMMARY:

Max Uncertainty : 0,045160 [%]
Max Uncertainty : 0,073086 [kPa]
RSQ : 1,000000
Calibration points : 28

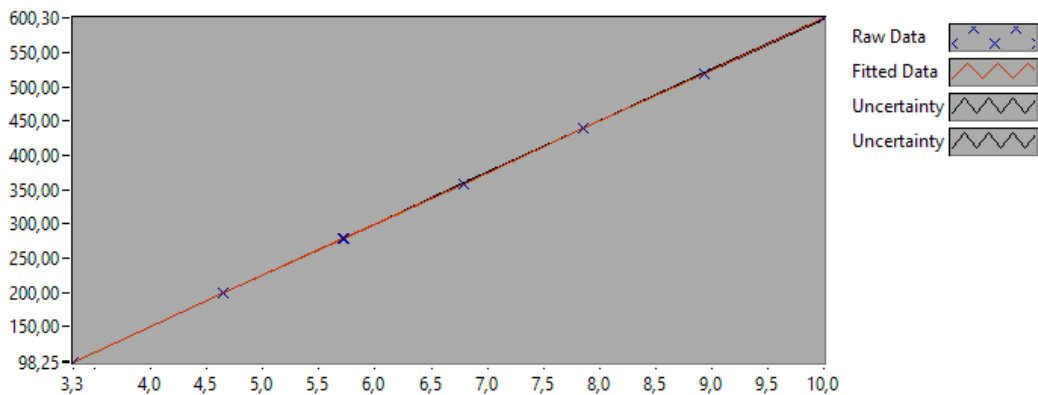


Figure 1 : Calibration chart (The uncertainty band is multiplied by 10)

Rakel Heggset

CALIBRATION VALUES

Value [kPa]	Voltage [V]	Best Poly. Fit [kPa]	Deviation [kPa]	Uncertainty [%]	Uncertainty [kPa]
<u>98,695989</u>	<u>3,316133</u>	<u>98,785989</u>	<u>-0,090000</u>	<u>0,045160</u>	<u>0,044571</u>
<u>198,847060</u>	<u>4,651285</u>	<u>198,935900</u>	<u>-0,088840</u>	<u>0,019122</u>	<u>0,038024</u>
<u>278,967917</u>	<u>5,718195</u>	<u>278,964983</u>	<u>0,002934</u>	<u>0,013648</u>	<u>0,038073</u>
<u>359,088773</u>	<u>6,786206</u>	<u>359,076699</u>	<u>0,012074</u>	<u>0,011945</u>	<u>0,042892</u>
<u>439,209630</u>	<u>7,854869</u>	<u>439,237259</u>	<u>-0,027629</u>	<u>0,011649</u>	<u>0,051165</u>
<u>519,330487</u>	<u>8,923545</u>	<u>519,398783</u>	<u>-0,068296</u>	<u>0,011847</u>	<u>0,061524</u>
<u>599,451344</u>	<u>9,991658</u>	<u>599,518091</u>	<u>-0,066747</u>	<u>0,012191</u>	<u>0,073077</u>
<u>599,491344</u>	<u>9,991161</u>	<u>599,480833</u>	<u>0,010511</u>	<u>0,012189</u>	<u>0,073074</u>
<u>519,370487</u>	<u>8,922601</u>	<u>519,327958</u>	<u>0,042529</u>	<u>0,011845</u>	<u>0,061521</u>
<u>439,249630</u>	<u>7,853834</u>	<u>439,159582</u>	<u>0,090048</u>	<u>0,011649</u>	<u>0,051166</u>
<u>359,128773</u>	<u>6,785436</u>	<u>359,018944</u>	<u>0,109830</u>	<u>0,011943</u>	<u>0,042889</u>
<u>279,007917</u>	<u>5,718150</u>	<u>278,961624</u>	<u>0,046293</u>	<u>0,013644</u>	<u>0,038067</u>
<u>198,887060</u>	<u>4,650334</u>	<u>198,864626</u>	<u>0,022434</u>	<u>0,019127</u>	<u>0,038041</u>
<u>98,735989</u>	<u>3,314905</u>	<u>98,693875</u>	<u>0,042114</u>	<u>0,045153</u>	<u>0,044582</u>
<u>98,765989</u>	<u>3,316532</u>	<u>98,815922</u>	<u>-0,049933</u>	<u>0,045125</u>	<u>0,044568</u>
<u>198,917060</u>	<u>4,652721</u>	<u>199,043628</u>	<u>-0,126568</u>	<u>0,019114</u>	<u>0,038022</u>
<u>279,037917</u>	<u>5,719760</u>	<u>279,082387</u>	<u>-0,044470</u>	<u>0,013643</u>	<u>0,038070</u>
<u>359,158773</u>	<u>6,787402</u>	<u>359,166388</u>	<u>-0,007614</u>	<u>0,011943</u>	<u>0,042893</u>
<u>439,279630</u>	<u>7,855777</u>	<u>439,305365</u>	<u>-0,025735</u>	<u>0,011650</u>	<u>0,051175</u>
<u>519,400487</u>	<u>8,924320</u>	<u>519,456886</u>	<u>-0,056399</u>	<u>0,011846</u>	<u>0,061530</u>
<u>599,521344</u>	<u>9,992383</u>	<u>599,572506</u>	<u>-0,051162</u>	<u>0,012190</u>	<u>0,073084</u>
<u>599,521344</u>	<u>9,991957</u>	<u>599,540510</u>	<u>-0,019166</u>	<u>0,012191</u>	<u>0,073086</u>
<u>519,390487</u>	<u>8,923125</u>	<u>519,367247</u>	<u>0,023240</u>	<u>0,011846</u>	<u>0,061529</u>
<u>439,269630</u>	<u>7,854415</u>	<u>439,203176</u>	<u>0,066454</u>	<u>0,011649</u>	<u>0,051172</u>
<u>359,148773</u>	<u>6,785906</u>	<u>359,054147</u>	<u>0,094627</u>	<u>0,011942</u>	<u>0,042891</u>
<u>279,027917</u>	<u>5,717951</u>	<u>278,946693</u>	<u>0,081224</u>	<u>0,013642</u>	<u>0,038064</u>
<u>198,907060</u>	<u>4,650559</u>	<u>198,881445</u>	<u>0,025615</u>	<u>0,019122</u>	<u>0,038035</u>
<u>98,755989</u>	<u>3,315031</u>	<u>98,703358</u>	<u>0,052631</u>	<u>0,045140</u>	<u>0,044579</u>

COMMENTS:

The uncertainty is calculated with 95% confidence. The uncertainty includes the randomness in the calibrated instrument during the calibration, systematic uncertainty in the instrument or property which the instrument under calibration is compared with (dead weight manometer, calibrated weights etc.), and due to regression analysis to fit the calibration points to a linear calibration equation. The calculated uncertainty can be used as the total systematic uncertainty of the calibrated instrument with the given calibration equation.

CALIBRATION REPORT

CALIBRATION PROPERTIES

Calibrated by: Rakel Heggset
Type/Producer: GE Druck
SN: 1195740
Range: 0-30 bar
Unit: kPa

CALIBRATION SOURCE PROPERTIES

Type/Producer: Pressurements deadweight tester P3223-1
SN: 66256
Uncertainty [%]: 0,01

POLY FIT EQUATION:

$Y = -748,02836706E+0X^0 + 374,74033293E+0X^1$

CALIBRATION SUMMARY:

Max Uncertainty : 0,474712 [%]
Max Uncertainty : 0,610615 [kPa]
RSQ : 0,999999
Calibration points : 32

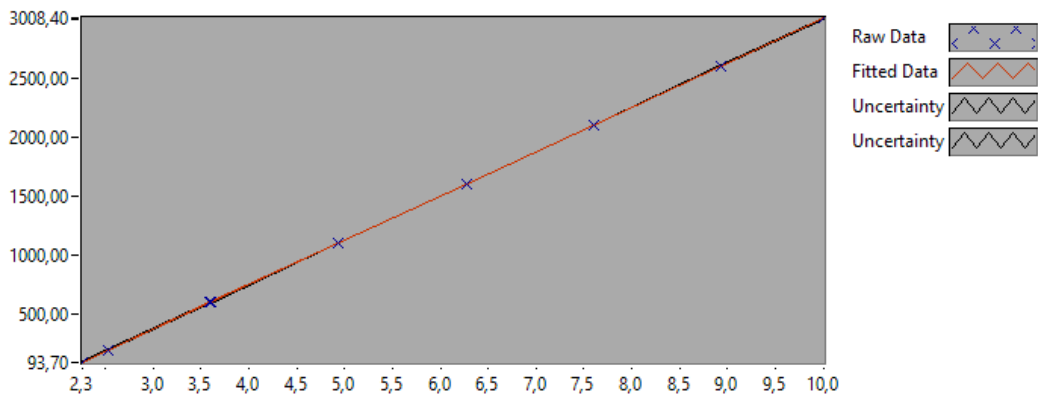


Figure 1 : Calibration chart (The uncertainty band is multiplied by 10)

Rakel Heggset

CALIBRATION VALUES

Value [kPa]	Voltage [V]	Best Poly Fit [kPa]	Deviation [kPa]	Uncertainty [%]	Uncertainty [kPa]
<u>98,766005</u>	<u>2,258740</u>	<u>98,412571</u>	<u>0,353434</u>	<u>0,474686</u>	<u>0,468828</u>
<u>198,917076</u>	<u>2,525077</u>	<u>198,219894</u>	<u>0,697182</u>	<u>0,224909</u>	<u>0,447382</u>
<u>599,521360</u>	<u>3,595452</u>	<u>599,332667</u>	<u>0,188693</u>	<u>0,062198</u>	<u>0,372889</u>
<u>1100,276715</u>	<u>4,934374</u>	<u>1101,080491</u>	<u>-0,803777</u>	<u>0,029157</u>	<u>0,320811</u>
<u>1601,032069</u>	<u>6,273150</u>	<u>1602,774090</u>	<u>-1,742020</u>	<u>0,020864</u>	<u>0,334044</u>
<u>2101,787424</u>	<u>7,606347</u>	<u>2102,376673</u>	<u>-0,589249</u>	<u>0,019317</u>	<u>0,405992</u>
<u>2602,542779</u>	<u>8,940240</u>	<u>2602,239981</u>	<u>0,302797</u>	<u>0,019689</u>	<u>0,512418</u>
<u>3003,147062</u>	<u>10,007798</u>	<u>3002,297351</u>	<u>0,849712</u>	<u>0,020333</u>	<u>0,610615</u>
<u>3003,137062</u>	<u>10,007453</u>	<u>3002,167996</u>	<u>0,969066</u>	<u>0,020331</u>	<u>0,610578</u>
<u>2602,532779</u>	<u>8,939781</u>	<u>2602,068057</u>	<u>0,464722</u>	<u>0,019688</u>	<u>0,512380</u>
<u>2101,777424</u>	<u>7,605981</u>	<u>2102,239351</u>	<u>-0,461927</u>	<u>0,019315</u>	<u>0,405960</u>
<u>1601,022069</u>	<u>6,272725</u>	<u>1602,614651</u>	<u>-1,592582</u>	<u>0,020864</u>	<u>0,334044</u>
<u>1100,266715</u>	<u>4,933826</u>	<u>1100,875237</u>	<u>-0,608522</u>	<u>0,029159</u>	<u>0,320828</u>
<u>599,511360</u>	<u>3,594993</u>	<u>599,160332</u>	<u>0,351028</u>	<u>0,062204</u>	<u>0,372919</u>
<u>198,907076</u>	<u>2,524762</u>	<u>198,101706</u>	<u>0,805370</u>	<u>0,224932</u>	<u>0,447406</u>
<u>98,756005</u>	<u>2,259001</u>	<u>98,510485</u>	<u>0,245520</u>	<u>0,474712</u>	<u>0,468807</u>
<u>98,766005</u>	<u>2,259097</u>	<u>98,546501</u>	<u>0,219505</u>	<u>0,474656</u>	<u>0,468799</u>
<u>198,917076</u>	<u>2,524903</u>	<u>198,154760</u>	<u>0,762316</u>	<u>0,224915</u>	<u>0,447395</u>
<u>599,521360</u>	<u>3,595123</u>	<u>599,209088</u>	<u>0,312272</u>	<u>0,062201</u>	<u>0,372910</u>
<u>1100,276715</u>	<u>4,933931</u>	<u>1100,914601</u>	<u>-0,637886</u>	<u>0,029159</u>	<u>0,320832</u>
<u>1601,032069</u>	<u>6,272741</u>	<u>1602,620798</u>	<u>-1,588728</u>	<u>0,020866</u>	<u>0,334068</u>
<u>2101,787424</u>	<u>7,606182</u>	<u>2102,314835</u>	<u>-0,527411</u>	<u>0,019316</u>	<u>0,405982</u>
<u>2602,542779</u>	<u>8,939738</u>	<u>2602,052183</u>	<u>0,490596</u>	<u>0,019688</u>	<u>0,512389</u>
<u>3003,147062</u>	<u>10,007487</u>	<u>3002,180551</u>	<u>0,966512</u>	<u>0,020332</u>	<u>0,610603</u>
<u>3003,147062</u>	<u>10,007424</u>	<u>3002,157047</u>	<u>0,990016</u>	<u>0,020331</u>	<u>0,610584</u>
<u>2602,542779</u>	<u>8,939658</u>	<u>2602,021947</u>	<u>0,520832</u>	<u>0,019688</u>	<u>0,512378</u>
<u>2101,787424</u>	<u>7,605922</u>	<u>2102,217426</u>	<u>-0,430002</u>	<u>0,019316</u>	<u>0,405973</u>
<u>1601,032069</u>	<u>6,272704</u>	<u>1602,606836</u>	<u>-1,574766</u>	<u>0,020866</u>	<u>0,334066</u>
<u>1100,276715</u>	<u>4,933504</u>	<u>1100,754440</u>	<u>-0,477725</u>	<u>0,029160</u>	<u>0,320837</u>
<u>599,521360</u>	<u>3,594970</u>	<u>599,151772</u>	<u>0,369588</u>	<u>0,062203</u>	<u>0,372919</u>
<u>198,917076</u>	<u>2,524804</u>	<u>198,117668</u>	<u>0,799409</u>	<u>0,224919</u>	<u>0,447402</u>
<u>98,766005</u>	<u>2,258680</u>	<u>98,389980</u>	<u>0,376025</u>	<u>0,474691</u>	<u>0,468833</u>

COMMENTS:

The uncertainty is calculated with 95% confidence. The uncertainty includes the randomness in the calibrated instrument during the calibration, systematic uncertainty in the instrument or property which the instrument under calibration is compared with (dead weight manometer, calibrated weights etc.), and due to regression analysis to fit the calibration points to a linear calibration equation. The calculated uncertainty can be used as the total systematic uncertainty of the calibrated instrument with the given calibration equation.

Appendix - B

Results

B.1 Pressure drop in 90° bend

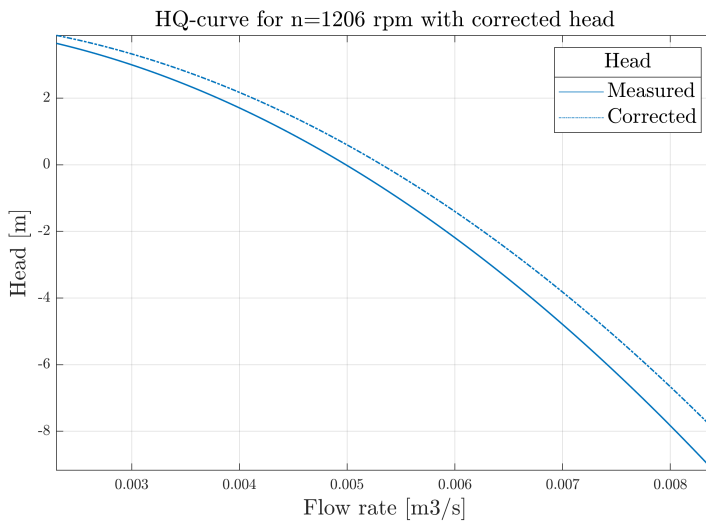


Figure B.1: Comparison of HQ-curves with measured outlet pressure vs. corrected pressure for 1206rpm.

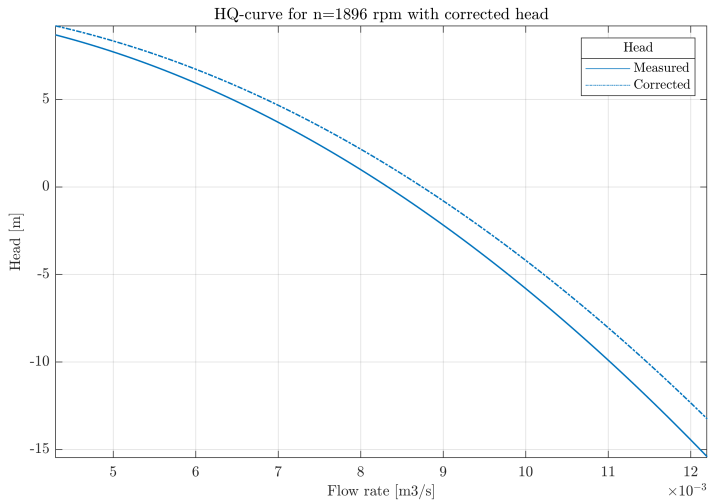


Figure B.2: Comparison of efficiency with measured outlet pressure vs. corrected pressure for $1896rpm$.

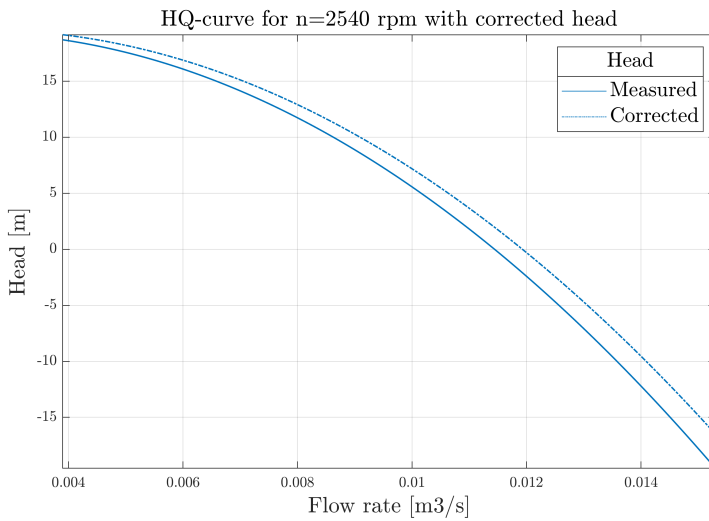


Figure B.3: Comparison of efficiency with measured outlet pressure vs. corrected pressure for $2176rpm$.

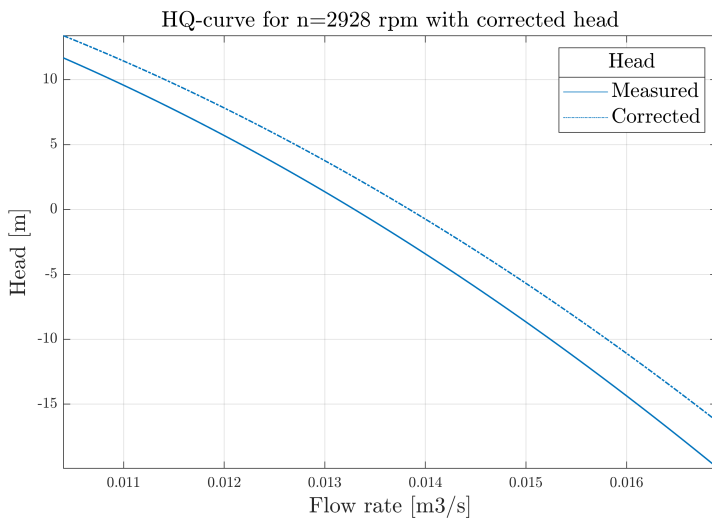


Figure B.4: Comparison of efficiency with measured outlet pressure vs. corrected pressure for 2928rpm.

Appendix - C

Uncertainty analysis

C.1 Uncertainty in the calibration

C.1.1 Uncertainty in the calibration of flow meter

The relative *systematic* uncertainty components from the calibration procedure is denoted f_{Q_a} and are listed below.

- $f_{Q_{\Delta W}} = \pm 0.05043\%$, the systematic uncertainty of the weight cells [16].
- $f_{Q_{divider}} = \pm 0.072611\%$, the systematic uncertainty of the divider [16].
- $f_{Q_{\rho}} = \pm 0.01\%$, the systematic uncertainty for calculating the water density [12].

With the RSS-method, the total systematic uncertainty for the calibration of the flow meter is

$$f_{Q_a} = \pm \sqrt{(f_{Q_{\Delta W}})^2 + (f_{Q_t})^2 + (f_{Q_{\rho}})^2} = \pm 0.0889\% \quad (\text{C.1})$$

The relative *random* uncertainty components from the calibration procedure is denoted f_{Q_b} and are listed below.

- $f_{Q_{\Delta W}} = 0.00007\pm$, the random uncertainty of the weight cells found with the Student-t distribution.
- $f_{Q_{divider}} = \pm 0.050339\%$, the random uncertainty of the divider [16].

Again, using the RSS-method, the total random uncertainty for the calibration of the flow meter is

$$f_{Q_b} = \pm \sqrt{(f_{Q_{\Delta W}})^2 + (f_{Q_{divider}})^2} = \pm 0.0503\pm \quad (\text{C.2})$$

C.1.2 Uncertainty in the calibration of torque transducer

The calibration of the torque transducer only consist of systematic uncertainties, as the neither the arm or the weights have a random component. The uncertainties are listed below.

- $f_{T_{arm}} = \pm 0.02\%$, the relative uncertainty of the length of the lever arm. The arm was measure to be $L = 0.5m$ with a ruler of an absolute uncertainty of $\pm 0.0001m$.
- $f_{T_{weights}} = \pm 0.003\%$, the relative uncertainty of the $5kg$ weights. The absolute uncertainty of the weights is $\pm 0.15g$.
- $f_{T_{fixture}} = \pm 0.0106\%$, the relative uncertainty of the fixture weight. The mass of the fixture was measured to be $4.7295kg$ with a weight of an absolute uncertainty of $\pm 0.5g$.

The total uncertainty of the mass attached to the lever arm is found by combining the relative uncertainty of the weights and the fixture using the RSS-method

$$f_{T_W} = \pm \sqrt{(f_{T_{weights}})^2 + (f_{T_{fixture}})^2} = \pm 0.0110\% \quad (\text{C.3})$$

C.2 Uncertainty in the measurements

C.2.1 Uncertainty of the hydraulic efficiency

The uncertainty of the measured mechanical power was calculated using the uncertainties from the measured rotational speed and the torque. With $f_T = \pm 0.1574\%$ and $f_n = \pm 0.025\%$, f_P was found to be

$$f_P = \pm \sqrt{(f_T)^2 + (f_n)^2} = \pm 0.1594\% \quad (\text{C.4})$$

The uncertainty of the energy is found with Equation C.5, assuming that the con-

tribution from the uncertainty of the height difference $z_2 - z_1$ is negligible [16].

$$f_E = \pm \frac{e_E}{E} = \left(\frac{\sqrt{\left(\frac{e_{p_1}}{\bar{\rho}}\right)^2 + \left(\frac{e_{p_2}}{\bar{\rho}}\right)^2 + \left(\frac{e_{v_1}^2}{2}\right)^2 + \left(\frac{e_{v_2}^2}{2}\right)^2}}{\frac{p_2 - p_1}{\bar{\rho}} + \frac{v_2^2 - v_1^2}{2}} \right) \quad (\text{C.5})$$

The uncertainty of the velocity components in Equation C.5 is defined by Equation C.6, where $f_A = \pm 0.01\%$ is the uncertainty of the inlet and outlet pipe area, given by the manufacturer. Further, by defining the velocities as $v = Q/A$ the absolute error component of the velocities can be written as in Equation C.7.

$$f_{v_i} = \sqrt{f_Q^2 + f_{A_i}^2} = \pm 0.5916\% \quad (\text{C.6})$$

$$\frac{e_{v_i}^2}{2} = v_i^2 \cdot f_{v_i} \quad (\text{C.7})$$

With the inlet and outlet velocities for the best efficiency point being $v_1 = 1.47\text{m/s}$ and $v_2 = 6.75\text{m/s}$, respectively, the uncertainty for the hydraulic energy was found to be $f_E = \pm 0.3993\%$.

Appendix - D

Procedure for running the Centrifugal Pump Test Rig

D.1 General

This procedure describes how to run the Centrifugal Pump Test rig at the Waterpower Laboratory at NTNU. The water from the lower water reservoir is fed to the system by the pump in the basement into the pressure tank, through the centrifugal pump and back to the lower water reservoir.

In this procedure, some descriptions are given with a reference to an associated image. All the images may be found in section D.4.

D.2 The system

D.2.1 Description

The system in use is the Centrifugal Pump Test Rig. It is installed with numerous calibrated instruments connected to a data acquisition system and a specialized LabView program to record and compute necessary data. All installations and calculations are performed according to the IEC 60193 standard.

D.2.2 Equipment used for testing

- The pipe and pumping system facilities at the Waterpower Laboratory
- The Centrifugal Pump Test Rig
- GE Druck absolute pressure transducers
- Optiflux 2300C Ø100 electromagnetic flow meter with IFC 300 signal converter

- HBM T10F torque transducer
- Optical rotation counter
- Data acquisition unit and logging program created in LabView

D.3 Operation

D.3.1 Initial setting of the pipe system

Table D.1 on the last page shows an overview of the all the valves involved in the piping system. Make sure to close or open the valves as described

D.3.2 Preparations

Setting up the system

1. Turn on the ventilation fans. See Figure D.1(a).
2. Turn on the variable frequency drive for the feeding pump in the basement. Turn the switch to *Start*, and let it return to position 1. See Figure D.1(b).
3. Ensure that the bleed valve on the pressure tank is open.
4. Inspect the rig for any obstacles.
5. Make sure all instrumentation has power supply and are connected to a logging computer. The flow meter has a separate power supply, make sure it is connected.

Starting the pump and filling the pressure tank

1. Check that the pipe waterway is set as described in Table D.1.
2. Start the pump in the basement at 100 RPM and increase the speed with a few increments to 330 RPM to start filling the pressure tank. It is important that the feed pump is set to Turbine mode and **not** Pump mode. At 330 RPM the tank is filled to approximately the line marked on the surveillance screen in the control room.
3. Check the pump seals in the basement. There should be at least one drop every 20 seconds and no continuous flow. If in doubt contact the lab technicians. This water cools the seal packing. Close the bleed valve on top of the pressure tank when desired level is reached.

4. When the maximum water level is reached in the pressure tank, close the manual bleed valve on top of the tank.

Starting the engine

1. Turn on the engine power supply as shown in Figure D.2(a).
2. Make sure the switch for controlling the rotational speed is rotated all the way to the left (*0rpm*) and that "Driftsvender" is set to "Pumpedrift". Turn on the ignition by switching the key to the right and push the green on-button. Slowly turn the switch for rotational speed in the clockwise direction to increase the speed. See Figure D.2(b).

D.3.3 Run the test

The main goal with the centrifugal pump test rig is to measure the hydraulic pump efficiency and obtain the HQ-curve to describe the pump behaviour at different flow rates. This measurement procedure describes how to measure one curve for a constant rotational speed. To obtain several curves, repeat the steps for a new rotational speed.

Measuring the HQ-curve

1. Set the centrifugal pump to a constant rotational speed by turning the switch on the engine control unit.
2. Adjust the RPM of the feed pump in the basement to obtain the desired inlet pressure supplied by the pressure tank. Make sure it is high enough to avoid cavitation noise at the inlet pipe.
3. With the manual valve on the outlet pipe fully open, record the first data point with a recording time of 30 seconds.
4. Choke the valve with a small increment to reduce the flow rate.
5. Check the inlet pressure. In case of change, adjust the RPM of the feed pump to keep the inlet pressure constant.
6. Record the next data point.
7. Repeat step 4-6 until minimum possible flow rate.

D.3.4 Shut down

Turning off engine

1. Slowly turn down the rotational speed.
2. Turn of the ignition.
3. Turn off the power supply for the engine. See Figure D.2(a).

Draining the pressure tank

1. Decrease the feed pump to 330 RPM.
2. When the pressure is close to 0 in the pressure tank, open the manual bleeding valve on top of the tank.
3. Slowly decrease the RPM of the feed pump to 100 RPM.
4. Fully open the manual valves at the outlet pipe of the test rig if they are not already open.
5. Check the level of the pressure tank. When it's below 25%, stop the pump in the basement.
6. Wait until the water stops going through the centrifugal pump.

Shutting down

1. Turn of the ventilation fans.
2. Turn of the frequency drive in the basement.
3. Do an inspection round in the lab and around the pump in the basement.

Emergency shut down

The rig is shut down with the red button on the control panel. The button will stop the engine. In case of high leakage flow, close the manual valve located over the rig. This will stop all water going into the pump.

D.4 Figures

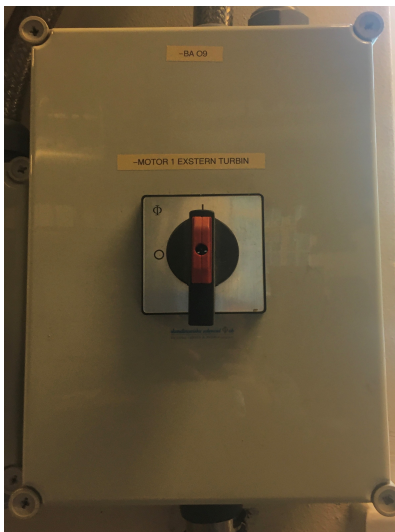


(a) Ventilation fan.



(b) Frequency drive for feed pump.

Figure D.1: Ventilation and frequency drive.



(a) Power supply.



(b) Engine control unit.

Figure D.2: Starting the engine.



(a) Manual valve on inlet pipe.



(b) Manual valve at the outlet pipe.

Figure D.3: Valves



Figure D.4: Manual valve on lower part of the pressure tank

Valves	Status
V1, To weight tank	Closed
V2, Draft tube tank to weight tank	Closed
V3, Draft tube tank outlet	Closed
V4	Closed
V5, Inlet pressure tank	Open
V6, To attic	Closed
V7, From attic	Closed
V8, Pressure tank	Closed
V9, Francis rig inlet	Closed
V10, Return to pump	Closed
V12, To sump	Open
V13, Inlet feed pump	Open
V12, To sump	Open
V13, Inlet feed pump	Open
V14	Closed
V15, Outlet feed pump	Open
V16	Closed
V17	Closed
V18, To sump	Open
V27, Draft tube tank air valve	Closed
V29, Auxilary rigs valve	Closed
Manual valve after pressure tank. Figure D.4.	Open
Manual bleed valve on top of the pressure tank.	Open
Manual valve on inlet pipe. Figure D.3(a).	Open
Manual valve on the outlet pipe. Figure D.3(b).	Open
Other valves connected to the waterway	Closed

Table D.1: Status for valves in the pipe system before starting procedure.

Appendix - E

Procedure for 3D printing

This is a procedure on how to perform 3D printing using the Original Prusa i3 MK3 3D printer available at the Waterpower Laboratory. On forehand, one must install the software PrusaSlicer to the computer.

1. Open the file for the object to be printed in the relevant CAD software. Save the file as a STL-file, describing the surface geometry of the object.
2. Open the STL-file in PrucaSlicer.
3. Add brim and skirt for the very first layers to assure that the filament properly attache to the printing surface.
4. Build up necessary support structure where the part has overhang.
5. Export the final construction as a G-code and save it to the memory card of the printer.
6. Before starting up the print, clean the surface of the printer with the recommended cleanser to remove fingerprints and dust.
7. Insert the memory card into the printer. Use the dashboard of the printer to choose which filament to use for printing.
8. Start the print.
9. Pay attention to the first layers of the printing. The filament may not attach properly to the plate and print must be restarted.
10. The print should be checked every now and then to see that the printer runs smoothly.

11. After the print is done, lift of the magnetic plate with the print and gently bend the plate to detach the printed object.
12. The support structure may be remove by hand or with a pair of small piers.

Appendix - F

MatLab codes

DataSort.m

```

1 %This script imports the .mat files with raw data and calculates the
  mean
2 %values for each recorded data point. The calibration constants are
  used
3 %to calculate real values and the head, hydraulic and mechanical
  power,
4 %and efficiency are calculated. The data is stored in a excel file.
5
6 %imports the file made with the TDMS converter
7 load('curve4.mat') %loading test data for one HQ curve at constant n
8 matSize = size(Measurements); %n rows and m columns
9 n = matSize(2); %nr of measured points along one curve for constant
  n
10
11 %make zero vectors for parameters
12 p1 = zeros(n,1);
13 p2 = zeros(n,1);
14 Torque = zeros(n,1);
15 Q = zeros(n,1);
16 rpm = zeros(n,1);
17
18 %mean values for each operational point
19 for i=1:n
20     p1(i) = mean(Measurements(i).P1.Values);
21     p2(i) = mean(Measurements(i).P2.Values);
22     Torque(i) = mean(Measurements(i).Torque.Values);
23     Q(i) = mean(Measurements(i).Flow.Values);
24     rpm(i) = mean(Measurements(i).RPM.Values);
25 end
26
27 %Converting to real values with calibration constants
28

```

```

29 %Calibration constans pressure
30 ap1 = 75.01014586; %kPascal
31 bp1 = -149.95763094; %kPascal
32 p1 = (p1.*ap1 + bp1).*10^3; %Pascal
33
34 ap2 = 374.74033293;
35 bp2 = -748.02836706;
36 p2 = (p2.*ap2 + bp2).*10^3; %Pascal
37
38 %Calibration constans torque
39 aT = 101.15407163;
40 bT = 975.79556026*10^-3;
41 Torque = (Torque.*aT + bT); %Nm
42
43 %Calibration constans flow
44 aQ = 0.002834;
45 bQ = -0.006306;
46 Q = Q.*aQ + bQ; %m^3/s
47
48 %RPM
49 rpm = rpm.*300; %rpm
50
51 %----Calculating parameters----%
52 rpm_e = mean(rpm); %rot. speed at engine shaft
53 rpm_i = rpm_e.*8; %rot. speed at impeller shaft
54
55 %Known parameters
56 rho = 1000; %density
57 dz = 0.08012; %in m
58 g = 9.82146516; %gravitation
59 D1 = 0.0722; %inlet diameter
60 D2 = 0.0443; %outlet diameter
61 A1 = pi*(D1^2)/4;
62 A2 = pi*(D2^2)/4;
63
64 dp = p2-p1; %pressure difference
65 c1 = Q./A1; %inlet velocity
66 c2 = Q./A2; %outlet velocity
67
68 %Find parameters
69 w = rpm_i.*pi/30; %angular velocity, in rad/s
70 Torque_i = Torque.*0.95/8; %assuming mechanical efficiency of 95%
71 Pm = Torque_i.*w; %mechanical power
72 H = dp./(rho*g) + (c2.^2-c1.^2)/(2*g) + dz; %head, in m
73 Ph = rho.*g*H.*Q; %hydraulic power
74 eta = (Ph./Pm).*100; %efficiency
75
76 %----Creating tables----%
77 %Creating table with new mean values
78 T = table(p1,p2,Torque,Q,rpm,H,Pm,Ph,eta);
79

```

```

80 Columns = table(p1,p2,Torque,Q,rpm,H,Pm,Ph,eta);
81 writetable(T,'curve4.xlsx') %write data matrix to excel file

```

HQplot.m

```

1 %This script plots the HQ-curve and the points obtained with
2 %the affinity laws.
3
4 M1 = xlsread('curve1.xlsx');
5 M1(5,:) = []; %not valid
6 M2 = xlsread('curve2.xlsx');
7 M3 = xlsread('curve3.xlsx');
8 M4 = xlsread('curve4.xlsx');
9 M5 = xlsread('curve5.xlsx');
10
11 Q1 = M1(:,4); H1 = M1(:,6); n1 = mean(M1(:,5))*8;
12 eta1 = M1(:,9); Hc1 = M1(:,10);
13 Q2 = M2(:,4); H2 = M2(:,6); n2 = mean(M2(:,5))*8;
14 eta2 = M2(:,9); Hc2 = M2(:,10);
15 Q3 = M3(:,4); H3 = M3(:,6); n3 = mean(M3(:,5))*8;
16 eta3 = M3(:,9); Hc3 = M3(:,10);
17 Q4 = M4(:,4); H4 = M4(:,6); n4 = mean(M4(:,5))*8;
18 eta4 = M4(:,9); Hc4 = M4(:,10);
19 Q5 = M5(:,4); H5 = M5(:,6); n5 = mean(M5(:,5))*8;
20 eta5 = M5(:,9); Hc5 = M4(:,10);
21
22 H1_fit = fit(Q1,H1,'poly2'); eta1_fit = fit(Q1,eta1,'poly2');
23 H2_fit = fit(Q2,H2,'poly2'); eta2_fit = fit(Q2,eta2,'poly2');
24 H3_fit = fit(Q3,H3,'poly2'); eta3_fit = fit(Q3,eta3,'poly2');
25 H4_fit = fit(Q4,H4,'poly2'); eta4_fit = fit(Q4,eta4,'poly2');
26 H5_fit = fit(Q5,H5,'poly2'); eta5_fit = fit(Q5,eta5,'poly2');
27
28 %Affinity laws %function [Q2,H2] = aff(H1,Q1,n1,n2)
29
30 %Affinitylaws based on n1
31 [Q2a1,H2a1] = aff(H1,Q1,n1,n2); %affinity laws for n2 based on n1
32 [Q3a1,H3a1] = aff(H1,Q1,n1,n3); %affinity laws for n3 based on n1
33 [Q4a1,H4a1] = aff(H1,Q1,n1,n4); %affinity laws for n4 based on n1
34 [Q5a1,H5a1] = aff(H1,Q1,n1,n5); %affinity laws for n5 based on n1
35
36 %Affinitylaws based on n2
37 [Q1a2,H1a2] = aff(H2,Q2,n2,n1); %affinity laws for n1 based on n2
38 [Q3a2,H3a2] = aff(H2,Q2,n2,n3); %affinity laws for n3 based on n2
39 [Q4a2,H4a2] = aff(H2,Q2,n2,n4); %affinity laws for n4 based on n2
40 [Q5a2,H5a2] = aff(H2,Q2,n2,n5); %affinity laws for n5 based on n2
41
42 %Affinitylaws based on n3
43 [Q1a3,H1a3] = aff(H3,Q3,n3,n1); %affinity laws for n1 based on n3
44 [Q2a3,H2a3] = aff(H3,Q3,n3,n2); %affinity laws for n2 based on n3
45 [Q4a3,H4a3] = aff(H3,Q3,n3,n4); %affinity laws for n4 based on n3

```

```

46 [Q5a3,H5a3] = aff(H3,Q3,n3,n5); %affinity laws for n5 based on n3
47
48 %Affinitylaws based on n4
49 [Q1a4,H1a4] = aff(H4,Q4,n4,n1); %affinity laws for n1 based on n4
50 [Q2a4,H2a4] = aff(H4,Q4,n4,n2); %affinity laws for n2 based on n4
51 [Q3a4,H3a4] = aff(H4,Q4,n4,n3); %affinity laws for n3 based on n4
52 [Q5a4,H5a4] = aff(H4,Q4,n4,n5); %affinity laws for n5 based on n4
53
54 %Affinitylaws based on n5
55 [Q1a5,H1a5] = aff(H5,Q5,n5,n1); %affinity laws for n1 based on n4
56 [Q2a5,H2a5] = aff(H5,Q5,n5,n2); %affinity laws for n2 based on n4
57 [Q3a5,H3a5] = aff(H5,Q5,n5,n3); %affinity laws for n3 based on n4
58 [Q4a5,H4a5] = aff(H5,Q5,n5,n4); %affinity laws for n5 based on n
59
60 %Creating vectors for Q and H from affinity points
61 Q1aff = [Q1a2' Q1a3' Q1a4' Q1a5']; H1aff = [H1a2' H1a3' H1a4' H1a5
        '];
62 Q2aff = [Q2a1' Q2a3' Q2a4' Q2a5']; H2aff = [H2a1' H2a3' H2a4' H2a5
        '];
63 Q3aff = [Q3a1' Q3a2' Q3a4' Q3a5']; H3aff = [H3a1' H3a2' H3a4' H3a5
        '];
64 Q4aff = [Q4a1' Q4a2' Q4a3' Q4a5']; H4aff = [H4a1' H4a2' H4a3' H4a5
        '];
65 Q5aff = [Q5a1' Q5a2' Q5a3' Q5a4']; H5aff = [H5a1' H5a2' H5a3' H5a4
        '];
66
67 H1aff_fit = fit(Q1aff',H1aff','poly2');
68 H2aff_fit = fit(Q2aff',H2aff','poly2');
69 H3aff_fit = fit(Q3aff',H3aff','poly2');
70 H4aff_fit = fit(Q4aff',H4aff','poly2');
71 H5aff_fit = fit(Q5aff',H5aff','poly2');
72
73 %BEP
74 n_BEP = 10000; Q_opt = 0.025; H_opt = 165;
75 [Q_BEP,H_BEP] = aff(H4,Q4,n4,n_BEP);
76 H_BEP_fit = fit(Q_BEP,H_BEP,'poly2');
77
78 %-----Plot curve
          -----%
79 %HQcurve
80 figure(1)
81 pl1 = plot(H1_fit,Q1,H1,'x');
82 hold on
83 pl2 = plot(H2_fit,Q2,H2,'o');
84 pl3 = plot(H3_fit,Q3,H3,'s');
85 pl4 = plot(H4_fit,Q4,H4,'^');
86 pl5 = plot(H5_fit,Q5,H5,'*');
87
88
89 %AFFINITY LAWS
90 %plotting affinitylaws for n1

```

```

91 plaff1 = plot(Q2a1,H2a1,'x',Q3a1,H3a1,'x',Q4a1,H4a1,'x',Q5a1,H5a1,'x
    ');
92 set(plaff1,'Color',[0, 0.4470, 0.7410])
93
94 %plottig affinitylaws for n2
95 plaff2 = plot(Q1a2,H1a2,'o',Q3a2,H3a2,'o',Q4a2,H4a2,'o',Q5a2,H5a2,'o
    ');
96 set(plaff2,'Color',[0.8510 0.3294 0.1020])
97
98 %plotting affinitylaws for n3
99 plaff3 = plot(Q1a3,H1a3,'s',Q2a3,H2a3,'s',Q4a3,H4a3,'s',Q5a3,H5a3,'s
    ');
100 set(plaff3,'Color',[0.9294 0.6902 0.1294])
101
102 %plottig affinity laws for n4
103 plaff4 = plot(Q1a4,H1a4,'^',Q2a4,H2a4,'^',Q3a4,H3a4,'^',...
104 Q5a4,H5a4,'^');
105 set(plaff4,'Color',[0.4902 0.1804 0.5608])
106
107 %plotting affinity laws for n5
108 plaff5 = plot(Q1a5,H1a5,'m*',Q2a5,H2a5,'m*',Q3a5,H3a5,'m*',...
109 Q4a5,H4a5,'m*');
110 set(plaff5,'Color',[0.4706 0.6706 0.1882])
111
112 %AFFINITYLAWS FIT CURVE
113 fit1 = plot(H1aff_fit,Q1aff,H1aff);
114 fit2 = plot(H2aff_fit,Q2aff,H2aff);
115 fit3 = plot(H3aff_fit,Q3aff,H3aff);
116 fit4 = plot(H4aff_fit,Q4aff,H4aff);
117 fit5 = plot(H5aff_fit,Q5aff,H5aff);
118 set([fit1(2) fit2(2) fit3(2) fit4(2) fit5(2)],'LineStyle','--')
119 set([fit1(1) fit2(1) fit3(1) fit4(1) fit5(1)],'Marker','none')
120 grid on
121 %setting colors and legends for HQ curves
122 set([pl1(1) pl1(2) fit1(2)],'Color',[0, 0.4470, 0.7410])
123 set([pl2(1) pl2(2) fit2(2)],'Color',[0.8510 0.3294 0.1020])
124 set([pl3(1) pl3(2) fit3(2)],'Color',[0.9294 0.6902 0.1294])
125 set([pl4(1) pl4(2) fit4(2)],'Color',[0.4902 0.1804 0.5608])
126 set([pl5(1) pl5(2) fit5(2)],'Color',[0.4706 0.6706 0.1882])
127 set([pl1 pl2 pl3 pl4 pl5], 'LineWidth', 1, 'MarkerSize', 8)
128
129 title('HQ-curve with fitted curve for affinity points')
130 xlabel('Flow rate [m3/s]')
131 ylabel('Head [m]')
132
133 LH(1) = plot(nan, nan, 'x-', 'Color', [0, 0.4470, 0.7410]);
134 LH(2) = plot(nan, nan, 'o-', 'Color', [0.8510 0.3294 0.1020]);
135 LH(3) = plot(nan, nan, 's-', 'Color', [0.9294 0.6902 0.1294]);
136 LH(4) = plot(nan, nan, '^-', 'Color', [0.4902 0.1804 0.5608]);
137 LH(5) = plot(nan, nan, '*-', 'Color', [0.4706 0.6706 0.1882]);
138 LH(6) = fit1(2); LH(7) = fit2(2); LH(8) = fit3(2);

```

```

139 LH(9) = fit4(2); LH(10) = fit5(2);
140
141 L{1} = '1206 rpm'; L{2} = '1896 rpm'; L{3} = '2176 rpm';
142 L{4}='2540 rpm'; L{5} = '2928 rpm';
143
144 %legend with affinity fit curves
145 % L{6} = 'Affinity for 1206 rpm'; L{7} = 'Affinity for 1896 rpm';
146 % L{8} = 'Affinity for 2176 rpm'; L{9} = 'Affinity for 2540 rpm';
147 % L{10} = 'Affinity for 2928 rpm';
148
149 %legend for rotatational speed
150 leg1 = legend(LH,L);
151 title(leg1,'Rotational speed (n)')
152
153 figure(3) %Efficiency
154 ple1 = plot(eta1_fit,Q1,eta1,'x');
155 hold on;
156 ple2 = plot(eta2_fit,Q2,eta2,'o');
157 ple3 = plot(eta3_fit,Q3,eta3,'s');
158 ple4 = plot(eta4_fit,Q4,eta4,'^');
159 ple5 = plot(eta5_fit,Q5,eta5,'*');
160
161 lg4 = legend(LH,L);
162 title(lg4,'Rotational speed (n)')
163 % ple6 = plot(Q1(5),18.7807,'o','Color',[0, 0.4470, 0.7410]);
164 % ple7 = plot(0.00595,50.8923,'o','Color',[0.8510 0.3294 0.1020]);
165 % ple8 = plot(0.007196,49.8847,'o','Color',[0.9294 0.6902 0.1294]);
166 % ple9 = plot(0.00693,65.3694,'o','Color',[0.4902 0.1804 0.5608]);
167 % ple10 = plot(Q5(4),42.3399,'o','Color',[0.4706 0.6706 0.1882]);
168
169 set(ple1,'Color',[0, 0.4470, 0.7410]);
170 set(ple2,'Color',[0.8510 0.3294 0.1020]);
171 set(ple3,'Color',[0.9294 0.6902 0.1294]);
172 set(ple4,'Color',[0.4902 0.1804 0.5608]);
173 set(ple5,'Color',[0.4706 0.6706 0.1882]);
174 set([ple1 ple2 ple3 ple4 ple5], 'LineWidth', 1, 'MarkerSize', 8)
175
176 xlabel('Flow rate [m3/s]');ylabel('Efficiency [-]');
177 title('Pump efficiency')
178 %xlim([0.002 0.014])
179 grid on;
180
181 %----Table for dH----%
182
183 % %errors for affinity laws based on n4
184 [e_Head1,f_Head1] = errorfunc(Q1a5,H1a5,H1_fit);
185 [e_Head2,f_Head2] = errorfunc(Q2a5,H2a5,H2_fit);
186 [e_Head3,f_Head3] = errorfunc(Q3a5,H3a5,H3_fit);
187 [e_Head4,f_Head4] = errorfunc(Q4a5,H4a5,H4_fit);
188 %
189 % T = table(e_Head1',e_Head2',e_Head3',e_Head4');

```



```
190 % Columns = table(e_Head1,e_Head2,e_Head3,e_Head4);
191 % writetable(T,'AbsoluteError_n5.xlsx') %write data matrix to excel
    file
```

